1-1-2015

The Study Of Ionization In A Military, Heavy-Duty, Diesel Engine

Steven Zielinski
Wayne State University,

THE STUDY OF IONIZATION IN A MILITARY, HEAVY-DUTY, DIESEL ENGINE

by

STEVEN ZIELINSKI

THESIS

Submitted to the Graduate School

of Wayne State University,

Detroit, Michigan

in partial fulfillment of the requirements

for the degree of

MASTER OF SCIENCE

2015

MAJOR: MECHANICAL ENGINEERING

Approved By:

_____

Advisor Date

DEDICATION

The beginning of this work is lovely dedicated to my parents. You invested your lives into me to teach me value of hard work. Your example and influence in my life developed life-long lessons that daily guide me in the decisions I make. From as long as I can remember, you encouraged and inspired me to do my best. Truly, the achievements that brought me to this point belong to you.

The completion of this work is lovely dedicated to my wife. Your patience, trust, and loving support were qualities I needed from you to finish my research. The joy you bring to my life gave me energy to move forward when I was tired and overwhelmed. My heart belongs to you. You are my greatest treasure.

ACKNOWLEDGEMENTS

To Dr. Naeim Henein, I want to express my deepest gratitude for your service to me as my advising professor. The enthusiasm with which you approach your research is incredibly contagious. I am truly privileged to have been your student. Your experience, knowledge, and intuition are inseparably represented in this work. My research and professional career have been greatly impacted by your vision for me to develop and grow. The opportunity to work with you has been invaluable.

To Eric Blash, thank you for your mentorship in my early days as an engineer. Had it not been for you, I would not have joined the research team as Wayne State University. Your work to set up Lab 1551 with a Caterpillar C7 for experimental testing was a great help to me.

To Tim Tappert, thank you for transforming rough sketches into machined works of art. Your partnership in developing instrumentation bores in the engine cylinder head made this research possible.

To Eric Gingrich, thank you for your help in writing MATLAB scripts for data processing. Your guidance and suggestions throughout the writing of this thesis were greatly appreciate and improved the quality of this work.

To my colleagues Prasad Raut and Kamal Asaad, thank you for the many hours spent working together to obtain experimental data from our research engine. Your friendship made the tiresome work enjoyable. Both of you express diligence and intelligence of which I deeply respect.

Thank you,

Steve

TABLE OF CONTENTS

DEDICATION ii

ACKNOWLEDGEMENTS iii

LIST OF FIGURES vii

LIST OF TABLES xi

INTRODUCTION 1

CHAPTER 1.0 : LITERATURE REVIEW OF IONIZATION 2

1.1 CHEMICAL REACTIONS 2

1.2 ION SENSOR 4

1.2.1 Operating Principles 4

1.2.2 Location 6

1.2.3 Sensor Tip Length and Shape 7

1.3 TEST RESULTS 10

1.4 CONCLUSION 29

CHAPTER 2.0 : MODERN FUEL INJECTION EQUIPMENT 30

2.1 HYDRAULIC-ELECTRONIC UNIT INJECTION 30

2.2 HIGH-PRESSURE COMMON RAIL 34

2.3 MAJOR VARIABLES OF THE MODERN FUEL INJECTION SYSTEM 38

2.3.1 Injection Pressure 38

2.3.2 Injection Rate Shaping 40

2.3.3 Multiple Injections 42
2.4 CONCLUSION 44
CHAPTER 3.0 : EXPERIMENTAL SETUP 45
3.1 TEST BED 45
3.1.1 Engine 45
3.1.2 Dynamometer 45
3.2 DATA ACQUISITION SYSTEM 46
3.2.1 Overview 46
3.2.2 Low-Speed 47
3.2.3 High-Speed 48
3.3 HARDWARE MODIFICATIONS 48
3.4 ION SENSOR DESIGN 51
3.4.1 Glow Plug Ion Sensor 51
CHAPTER 4.0 : EXPERIMENTAL DATA AND ANALYSIS 53
4.1 DESCRIPTION OF MEASUREMENT CONDITIONS 53
4.1.1 Data Sampling and Presentation 53
4.1.2 Engine Operating Mode 53
4.1.3 Description of Example Data 54
4.2 EFFECT OF ZERO-SHIFT 57
4.3 FUEL INJECTOR ION CURRENT CHARACTERISTICS 59
4.3.1 Ion Current as a Fuel Injection System Diagnostic 60

4.3.2 Effect of Engine Load on Ion Current 62

4.4 GLOW PLUG ION CURRENT CHARACTERISTICS 65

4.4.1 Effect of Injection Timing on Ion Current 65

4.4.2 Effect of Engine Load on Ion Current 69

4.4.3 Comparison of SOIC to RHR 71

CHAPTER 5.0 : CONCLUSIONG AND RECOMMENDATION FOR FUTURE WORK 75

APPENDIX A 77

APPENDIX B 79

REFERENCES 80

ABSTRACT 84

AUTOBIOGRAPHICAL STATEMENT 85

LIST OF FIGURES

Figure 1.1: Modified glow plug for ionization [11] 4

Figure 1.2: Electrical Diagram of Ion Sensing Glow Plug [3] 5

Figure 1.3: Offset Due to Soot Build Up on Sensing Tip [6] 5

Figure 1.4: Electrical Diagram of Ion Sensing Fuel Injector [5] 6

Figure 1.5: Four Ion Sensors in the Same Cylinder [2] 7

Figure 1.6: Ion Sensor Experimental Tips [8] 8

Figure 1.7: Effect of Polarity and Voltage Level on Ion Current [8] 9

Figure 1.8: Effect of Polarity and Voltage Level on Ion Current [6] 10

Figure 1.9: (1 of 5 test points) 1500 RPM, 32 Nm load [1] 11

Figure 1.10: Detection of Pilot Injection with Ion Current [1] 11

Figure 1.11: Effect of EGR Sweep on Ion Current [1] 12

Figure 1.12: Fuel Properties Affect on Ion Current [6] 12

Figure 1.13: Effect of Swirl Ratio on Ion Current Signal [2] 13

Figure 1.14: EGR Sweep Without Pilot Injection [2] 14

Figure 1.15: EGR Sweep with Pilot Injection [2] 14

Figure 1.16: Correlation of EGR Percentage to Ion Current Amplitude [2] 15

Figure 1.17: Offset Between the Different Methods of Finding SOC [2] 15

Figure 1.18: Comparison of Standard Deviation [2] 16

Figure 1.19: Transient Comparison Between Burn Rate and Ion Current in Determining SOC [2] 17

Figure 1.20: Example of Four Ion Peaks in Diesel Engine [9] 18

Figure 1.21: Increase in Ion Current Due to Engine Load [9] 20

Figure 1.22: Multi-Sensing Fuel Injector Signal Compared Over a Successful Injection (blue) and Faulty Injection (red) [5] 20

Figure 1.23: Simulation of Ion Probe Sensitivity to Location [5] 21
Figure 1.24: Examples of Ion Current Features Studied for Correlation to Combustion Phasing [3] 21
Figure 1.25: Relation of SIC to LPPC with Variable Load and Injection Pressure [3] 22
Figure 1.26: Relation of SIC to LPPC with Variable Load and SOI Timing [3] 22
Figure 1.27: Variation of SIC and LPPC Under Open-Loop Control [3] 23
Figure 1.28: Variation of SIC and LPPC Under Closed-Loop Control [3] 23
Figure 1.29: Comparison of Measured and Estimated Soot with Varied Load and Injection Pressure. [17] 24
Figure 1.30: Comparison of Measured and Estimated Soot Under Constant Engine Load with Varied Engine Speed [17] 25
Figure 1.31: Comparison of Measured and Estimated Soot Under Constant Engine Speed and Load with Varied MAP [17] 25
Figure 1.32: Comparison of Ion Current with Varied Injection Pressure [6] 26
Figure 1.33: Ion Current Compared to NO at Cycle 8, 12, and 61 [10] 27
Figure 1.34: Relationship of Ion Current to Engine Load [6] 28
Figure 1.35: Correlation of Max Ion Current to NO and Soot Emissions [6] 29
Figure 2.1: Caterpillar HEUI System Diagram [19] 30
Figure 2.2: HEUI Fuel Injector 31
Figure 2.3: Caterpillar HEUI fuel injector [19] 32
Figure 2.4: Fill Scheme for Square Rate Shape [19] 33
Figure 2.5: Bosch CRI3 System Overview [21] 35
Figure 2.6: Bosch CRI3 fuel injector [21] 35
Figure 2.7: Bosch CRI3 internal components [22] 36
Figure 2.8: Control Valve Positions [22] 36

Figure 2.9: Preferred injection pressures based on engine speed and load [10] 39

Figure 2.10: Rate Shape Examples [29] 40

Figure 2.11: Optimal Rate Shape Engine Map [29] 41

Figure 2.12: Rate of Heat Release at 2200 RPM with 2 Nm Torque [31] 42

Figure 2.13: BSFC reduction with pre-injection and post-injection [33] 43

Figure 2.14: Result using two different ramp rates combined with multiple injections [34] 44

Figure 3.1: Engine and Dynamometer Setup 46

Figure 3.2: Overview of Data Acquisition System 47

Figure 3.3: Bottom Side of Cylinder Head 49

Figure 3.4: Top Side of Cylinder Head 50

Figure 3.5: Pressure Transducer Sleeve (Left) and Glow Plug Sleeve (Right) 51

Figure 3.6: Ion Current Glow Plug with Attached Wires 52

Figure 3.7:Ion Current Glow Plug with Brazed Rod 52

Figure 4.1: Soot Comparison for Optimized Injection Strategy [19] 54

Figure 4.2: 85 ft-lbs at 1000 RPM, Full Cycle 55

Figure 4.3: 85 ft-lbs at 1000 RPM, Expanded View 56

Figure 4.4: Example of Zero-Shift within a Test Point 58

Figure 4.5: Zero-Shift in Fuel Injector between Test Points 59

Figure 4.6: Zero-Shift in Glow Plug between Test Points 59

Figure 4.7: Comparison of Injection Command to Injector Ion Current Signal 60

Figure 4.8: Electrical Signature of Cylinder 5 and 6 62

Figure 4.9: Injector Ion Current at 1000 RPM 63

Figure 4.10: Overrun of Electrical Signature into Combustion 65

Figure 4.11: Change in Injection Timing with Engine Load 66

Figure 4.12 Change in Injection Duration with Engine Load 66

Figure 4.13: Delay in SOIC from SOI 68

Figure 4.14: Change in Cylinder Pressure with Engine Load 69

Figure 4.15: Change in Ion Current Amplitude with Engine Load 70

Figure 4.16: Relationship between Ion Current Amplitude and Cylinder Pressure 70

Figure 4.17 : RHR for Ion Current from Glow Plug 71

Figure 4.18: Amplitudes of LPPC and Diffusion Burn 72

Figure 4.19: Increase of Delay Between LPPC and SOIC 73

Figure 4.20: Delay in SOIC from LPPC 74

LIST OF TABLES

Table 3-1: CAT C7 Engine Characteristics 45

Table 4-1: Comparison of Injection Command to Fuel Injector Ion Current 61

Table 4-2: Offset in SOIC from SOI 68

INTRODUCTION

Over the past decade and into the foreseeable future, the demand for diesel engines to increase in fuel efficiency and decrease in exhaust emissions will continue. In order to progress in this endeavor, every minute function of the engine must be optimized. Although great time, effort, and money is spent on achieving optimal calibrations, the limit of what is obtainable is defined by the quantity and type of sensing equipment available to the engine control unit (ECU). Because of this, the automotive industry is constantly exploring the latest in sensing technology. Particularly of interest, sensors that can determine the operating conditions inside the cylinder are desired. While different sensors have emerged in this category, it has been primarily been dominated by the in-cylinder pressure transducer. Pressure transducers provide a great deal of information during the combustion process. Unfortunately, these sensors are expensive and can be difficult to integrate. An alternant solution to the in-cylinder pressure transducer is an ion sensor which is less expensive and can be integrated into standard diesel engine equipment such as the glow plug [1-4] or the fuel injector [5]. However, data gathered from ion sensors is not as consistent as pressure transducers and represents a localized measurement instead of the global conditions of the cylinder.

Over the past twenty years, much has been discovered about ionization. These studies suggest that ionization is a capable in-cylinder sensor worth considering. Most of these studies have been investigations into ionization using SI engines. While some characteristics of ionization are shared between SI and diesel engines, there are distinct differences. In this paper, the emphasis is ionization in diesel engines. However, when relevant, ionization data gathered from SI experiments is included.

CHAPTER 1.0 : LITERATURE REVIEW OF IONIZATION

1.1 CHEMICAL REACTIONS

Ionization in diesel engines is made of two primary stages, chemi-ionization and thermal ionization. Between the two, chemi-ionization is the dominant contributor to ion concentration. Unlike SI engines, the effects of thermal ionization usually cannot be distinguished from the ion current trace. The primary chemi-ionization reactions are considered to be (1) and (2) [1-2, 7-10].

$$CH + O \rightarrow CHO^+ + e^- \quad (1)$$

Although (1) is listed as the primary reaction, the reduction reaction, (2), produces more ions due to the faster reaction rate [1] and lower coefficient of recombination [7].

$$CHO^+ + H_2O \rightarrow H_3O^+ + CO \quad (2)$$

While there is basic agreement on the fundamental reactions producing ionization, there is a wide variety of opinions as to other contributing reactions.

In Glavmo et al. [1], their description of thermal ionization (3) is summarized by the following reaction where *M* represents a generic molecule, M^+ a positive generic ion, e^- an electron, and E_{ion} as the ionization energy.

$$M + E_{ion} \leftrightarrow M^+ + e^- \quad (3)$$

Also, the authors state that ions vanish due to recombination reactions. Essentially, free electrons combine with ions to form a stable molecule. The following reaction was given as an example of a recombination reaction:

$$H_3O^+ + e^- \rightarrow H_2O + H \quad (4)$$

Along with (1), Kubach et al. [2] list (5), which is the reaction of a hydrocarbon with an electron, as another primary reaction. This reaction is what they call “electron deposit”.

$$C_nH_x + e^- \rightarrow C_nH_x^- \quad (5)$$

In addition, they list (6), (7), and (8) as secondary ionization mechanisms and are classified respectively as proton-transfer, electron-transfer, and condensation reactions.

$$CHO^+ + CH_2 \rightarrow CH_3^+ + CO \quad (6)$$

$$O_2^- + C_nH_x \rightarrow C_nH_x^- \quad (7)$$

$$CH_3^+ + C_2H_2 \rightarrow C_3H_3^+ + H_2 \quad (8)$$

Lastly, two recombination reactions are given, electron impingement (9) and dissociating (10).

$$A^+ + e_{ionized}^- + e_{imping}^- \rightarrow A + e_{imping}^- \quad (9)$$

$$AB^+ + e^- \rightarrow A + B \quad (10)$$

While Henein et al. [9] list (1) and (2) as primary chemi-ionization reactions, they also list (11). Interestingly, they offer that (12) should be substituted in for (2) in the presence of rich and sooty hydrocarbon air flames.

$$CHO^+ + NO \rightarrow NO^+ + HCO \quad (11)$$

$$CH^+ + C_2H_2 \rightarrow C_3H_3^+ + e \quad (12)$$

Lastly, they list a recombination reaction similar to what we find in Glavmo et al. [1].

$$H_3O^+ + e^- \rightarrow 2H + OH \quad (13)$$

Estefanous et al. [10] divide the chemi-ionization effects into three categories which are neutral reactants, charge transfer, and recombination. In neutral reactants (1) and (14) are listed. Charge transfer reactions include (2), (15) and (16). Lastly, (4) is provided as a recombination reaction which was already noted by Glavmo et al. [1].

$$CH + C_2H_2 \leftrightarrow C_3H_3^+ + e^- \quad (14)$$

$$CHO^+ + CH_2 \leftrightarrow CH_3^+ + CO \quad (15)$$

$$CHO^+ + NO \leftrightarrow NO^+ + CHO \quad (16)$$

The authors also gave a reaction for thermal ionization which is also similar to Glavmo et al. [1].

$$M \leftrightarrow M^+ + e^- \quad (17)$$

Along with chemi-ionization and thermal ionization, Estefanous et al. [10] introduces a third mechanism for ionization, electron attachment. In this process, a neutral particle will bind with a free electron in the post flame period. This forms negative ions and is described by (18).

$$A + e^{-} + M \leftrightarrow A^{-} + M \tag{18}$$

In a more recent work, Henein et al. [6], restate the processes for ionization already mentioned in [9]. However, there is an addition to thermal ionization which accounts for the *NO* reaction at high combustion temperatures as seen in (19).

$$NO + M \rightarrow NO^{+} + e + M \tag{19}$$

1.2 ION SENSOR

1.2.1 Operating Principles

In this section, a detailed description for two different methods of ion sensing in diesel engines is given. While there are more than these two methods, the two discussed are the most promising. In addition, an understanding of other methods can be gathered from this description since they usually are only a slight variation from what is discussed here.

As was already mentioned, most researchers exploring ionization have done so using a modified glow plug. The essential modification is insulating the heating element from the glow plug body. *Figure 1.1* shows the internal parts of a design used by researchers at Wayne State University [11].

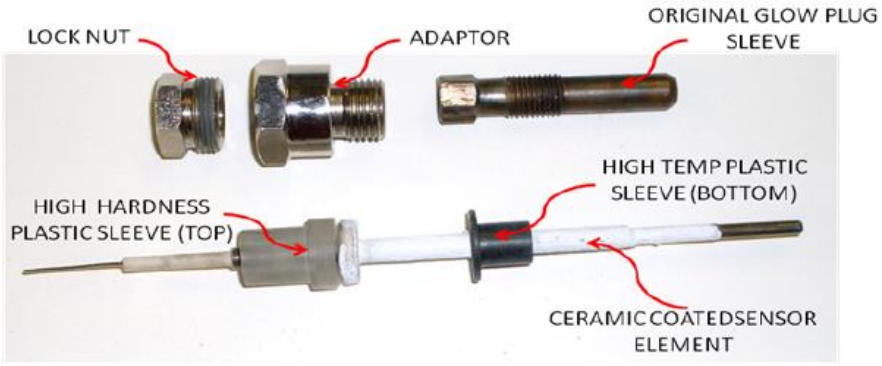

Figure 1.1: Modified glow plug for ionization [11]

Once the heating element is insulated, the metal glow plug tip serves as one electrode and the engine block serves as the other electrode to complete the circuit. In a slight variation of this method, an electrode actually protrudes outside of the glow tip [12]. In this case the electrode instead of the tip is used as the sensing element. An example of an electrical schematic for ion sensing glow plugs is presented in *Figure 1.2*.

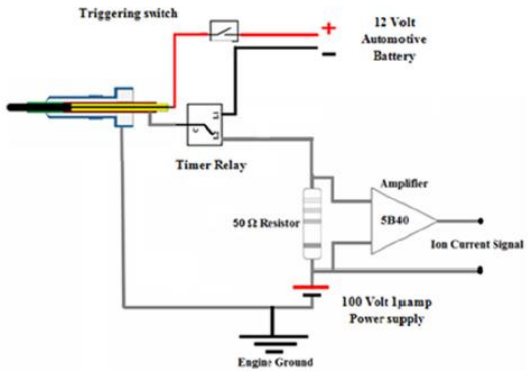

Figure 1.2: Electrical Diagram of Ion Sensing Glow Plug [3]

From the above diagram, it should be noticed that the heating function of the glow plug has been maintained. This is a major advantage that the glow plug ion sensor has over other ion sensors. Over time, the ion sensing tip builds a coating of soot. This coating causes an offset in the measured ion current as seen in *Figure 1.3*. However, the glow plug can be activated and the soot can be burned off resetting the offset back to zero.

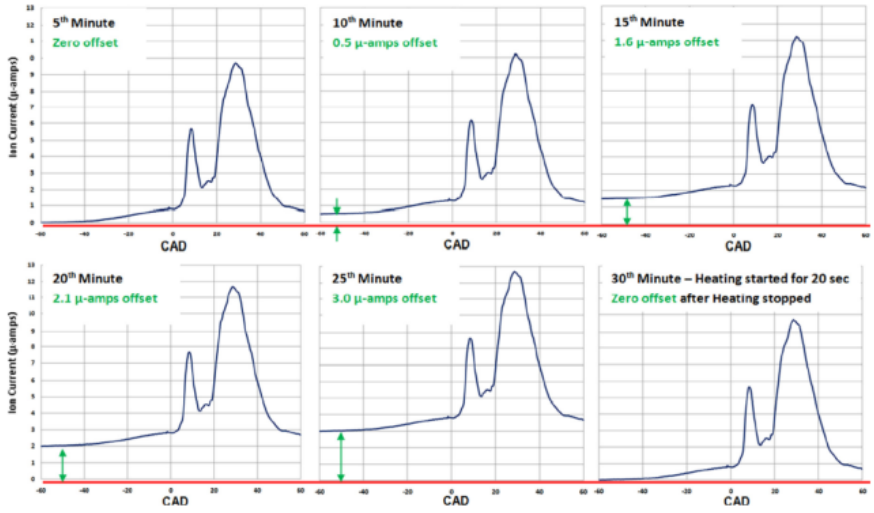

Figure 1.3: Offset Due to Soot Build Up on Sensing Tip [6]

In some diesel engines, there are no glow plugs and an air intake heater is used for cold-start conditions. These applications require another method for measuring ion current. Estefanous developed a method using the fuel injector itself [13]. In a common rail diesel engine, he was able to take ion current measurements by insulating the fuel rail and fuel injector from the engine block. A diagram of his circuit is shown in *Figure 1.4*.

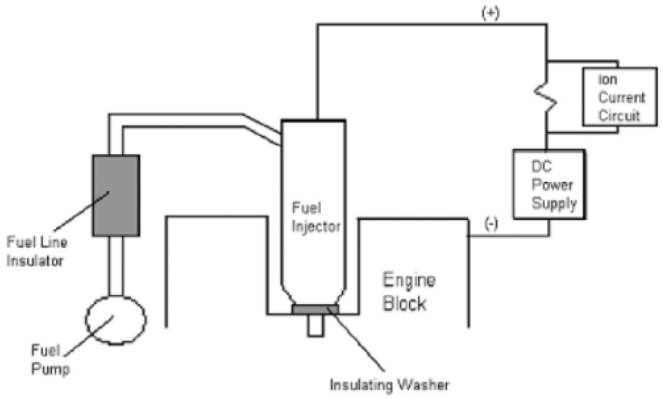

Figure 1.4: Electrical Diagram of Ion Sensing Fuel Injector [5]

1.2.2 Location

Arguably, the location of the ion sensor in diesel engines is less critical than it is in SI engines, although still important. According to Peron et al. [7], unless the ion sensor is close to the spark plug or the spark plug itself, it is not possible to distinguish between flame front and post flame front events. Since the spark begins combustion in an SI engine, it is possible and necessary to have the ion sensor directly in the location of the start of combustion. However, due to the heterogeneous charge of diesel engines, combustion does not start in a single location every time. In fact, combustion begins in several places in the cylinder simultaneously.

In diesel engines, several positions for the ion sensor have been tried. The most common position is through the glow plug bore [1-3]. Other methods include using the fuel injector itself [5] and installing custom ion current probes [2]. In Kubach et al., the effect of ion probe position was studied by placing four ion probes into a single cylinder. Probe 1 was located outside the piston bowl in the quench area. Probe 2 was located equidistant from the fuel injector as the glow plug bore, but near the intake valves.

Probe 3 was located at the edge of the piston bowl. Lastly, Probe 4 was located in the glow plug bore. *Figure 1.5* shows the configuration of the ion sensors.

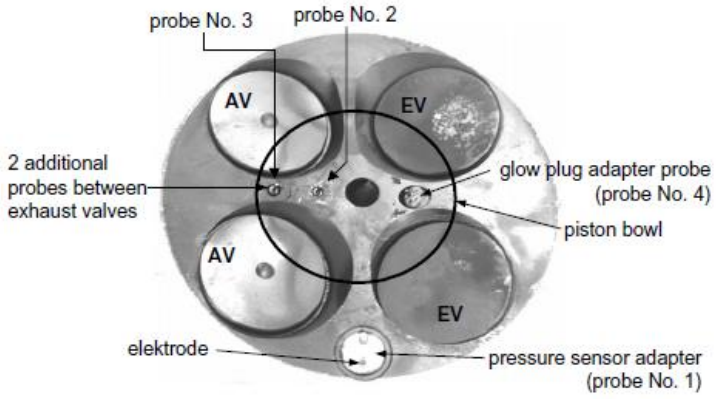

Figure 1.5: Four Ion Sensors in the Same Cylinder [2]

Before discussing the results, it is important to mention that of the four ion sensors, there were three different styles. Only Probe 2 and Probe 3 were identical in construction. However, the differences in their structure did not seem to be significant to the authors. The design for Probe 2 and Probe 3 left a very small air gap between the sensor's electrode and the cylinder head. This produced short circuits due to soot build up. The ion current from Probe 1 was barely detectable. The authors believed that the probe was too far away from the combustion flame. Probe 4 was the only location in which consistent measurements were possible. From this investigation, the authors suggest locating the probe in areas where soot is low, but yet close to the fuel injector.

1.2.3 Sensor Tip Length and Shape

Another study, Henein et al. [6], investigated the effects of penetration into the combustion bowl. Three different tip lengths were tested which ranged from 20.4 to 29.4 mm. It was demonstrated the longest tip produced the highest current amplitude. However, the shortest tip produced an ion current signal with more detail. This is because the longer probe averages the combustion conditions over the length of its penetration. The authors chose a medium tip length for conducting the rest of the experiments as a compromise between detail and amplitude.

Findings of Larsson et al. [8] agreed with Henein et al. [6]. Larsson investigated the impact of different tip shapes such as conical, spherical, and thin cylindrical discs. Tip penetration and tip surface area were also considered. *Figure 1.6* gives examples of the tips used.

Figure 1.6: Ion Sensor Experimental Tips [8]

The authors concluded that both surface area and penetration depth of the tip were significant factors in obtaining an ion current signal. The effect of tip shape did not seem to have any inherent impact other than when the tip shape changed the surface area or penetration.

1.2.4 Polarity and Voltage

In order for ion current to be generated, the ion sensors must be energized with high amounts of direct current (DC) voltage. Typically, this voltage is referred to as bias voltage. The polarity of the bias voltage can be either positive or negative. For a positive bias voltage, the ion sensor tip is considered the anode and the piston, cylinder walls, etc. are considered the cathode. With a negative bias voltage, the ion sensor tip is considered the cathode and the piston, cylinder walls, etc. are considered the anode. In the experiments of most researchers, positive bias voltage holds an advantage [1,3-6,8-10]. This is because negatively charged electrons have a high mobility and can be more easily attracted to a small anode [1,6,8]. Ions on the other hand, are heavier and move slower. Therefore, they benefit from having a large surface area to collect on the cathode.

Another benefit mentioned by Badawy et al. [6] is the signal to noise ratio is reduced. This disagrees with Larsson et al. [8] though.

However, there are legitimate reasons for using negative bias voltage. Kubach et al. [2] preferred the negative bias voltage because by drawing out the ions, they were able to measure just the gases in the near vicinity to the sensor.

Another proponent of negative bias voltage was Henein et al. [14-15]. Through their experiments were in a SI engine, they witnessed less variation in the ion current trace with negative bias voltage. However, the authors attributed this to flame front speed changes which is SI phenomena. Because of this, it is difficult to determine if negative bias voltage offers an advantage in diesel engines.

There is disagreement between Glavmo et al. [1] and Kubach et al. [2] if electrons or ions are contributing factor to ionization. This probably explains why they both chose different polarities.

Several researchers studied the effects of polarity and voltage level. In Larsson et al. [8], voltage was varied from -400 to 500 V. Data from their experiment is given in *Figure 1.7*.

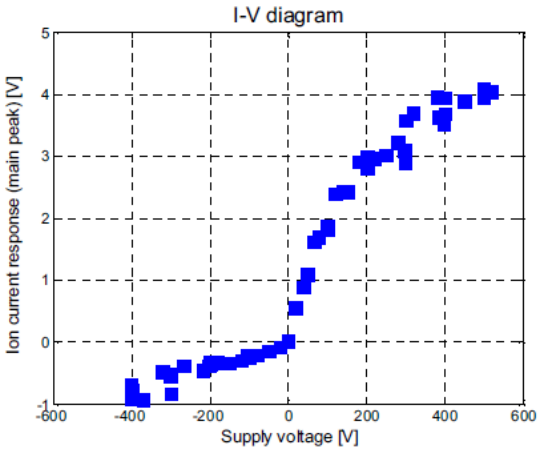

Figure 1.7: Effect of Polarity and Voltage Level on Ion Current [8]

From this test, it was established for further testing that positive bias voltage would be used. In addition, it was identified that after 250 V, there was diminishing returns on increasing the bias voltage to increase the peak ion current.

Confirming the study performed by Larsson [8], Henein et al. [6] conducted a similar experiment from -100 to 100 V. The positive polarity increased the amplitude of the ion current while the negative polarity did not. The results can be seen in *Figure 1.8*.

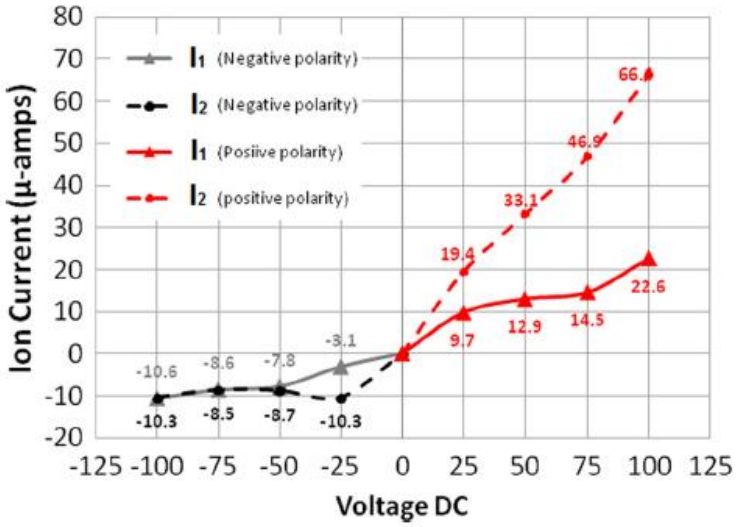

Figure 1.8: Effect of Polarity and Voltage Level on Ion Current [6]

1.3 TEST RESULTS

In the following section, a brief summary of the test results for several papers is provided. Real-world data is depicted and discussed.

Glavmo et al. [1] was one of first to extensively test ionization in diesel engines. The authors' first compared the ion current to the start of the main injection pulse. Five test points of increasing speed and varying load were chosen. At each test point, the start of the main injection pulse was varied three times with a step size of two CADs. 100 cycles of data were averaged in order to reduce the amount of fluctuation in the ion current signal. Although it is clearly demonstrated in *Figure 1.9* that ion current changes according to changes in the start of the main injection, the authors did not comment whether or not any feature of the ion current could be reliably correlated to a feature on the start of main injection curve.

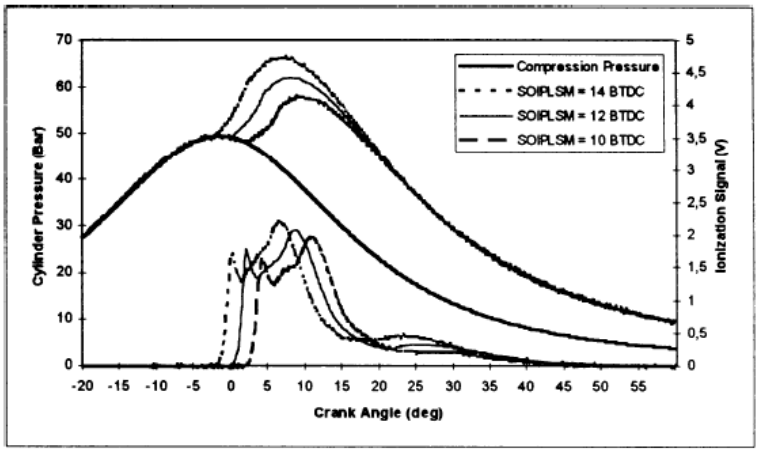

Figure 1.9: (1 of 5 test points) 1500 RPM, 32 Nm load [1]

Another set of tests were performed to investigate the detection of pilot injection. While keeping the main injection timing and total injected quantity (pilot + main) constant, the pilot injection timing and quantity were varied. This was compared to the case where no pilot injection was employed. Using the ionization signal, pilot injection was distinguishable from main injection. In addition, the ion current changed according to the changes in pilot injection. *Figure 1.10* summarizes the test points and compares ion current to the rate of heat release.

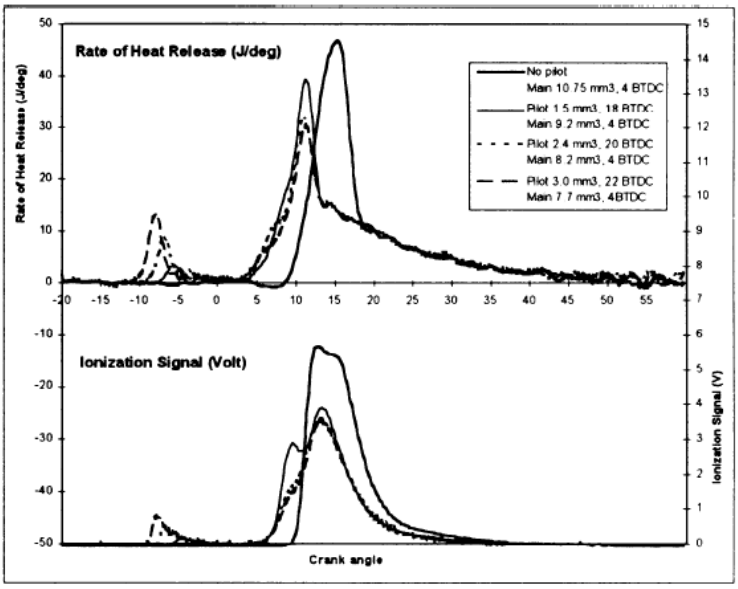

Figure 1.10: Detection of Pilot Injection with Ion Current [1]

Lastly, the effect of EGR was studied. The purpose of EGR is to reduce NOx formation by decreasing in-cylinder temperatures. In turn, the decreased temperatures reduced the ion current signal.

Since EGR is used on most diesel engines, it was important to demonstrate that ion current could still be useful under this condition. The authors ran of sweep of EGR percentages from 0-46% to show the effect on ion current. The results are displayed in *Figure 1.11*. Although the amplitude of the ion current signal was reduced, even under the highest EGR load of 46%, ion current was still detectable.

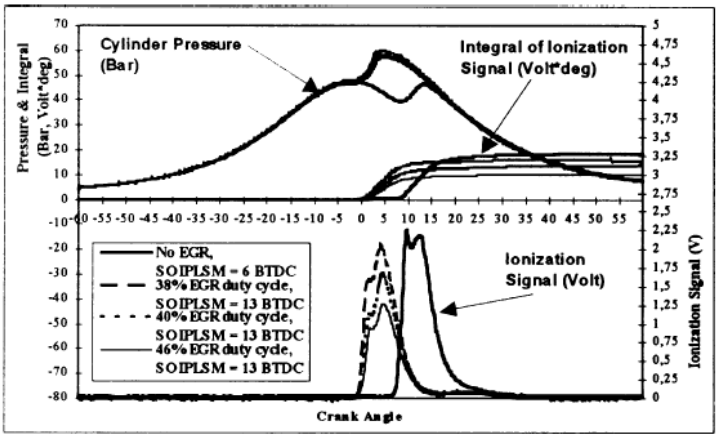

Figure 1.11: Effect of EGR Sweep on Ion Current [1]

In the literature, it was difficult to find any investigations involving diesel engines that study the effect of fuel properties or additives on ion current. In the absence of this data, a study conducted on a spark ignited engine will be substituted. In Peron et al. [6], a comparison between RON 98 unleaded fuel, leaded fuel, and propane is provided. From *Figure 1.12*, it was proven that fuel properties have an effect on ion current. However, the need for a relevant test on a diesel engine comparing diesel fuels, additives, and cetane numbers is still necessary.

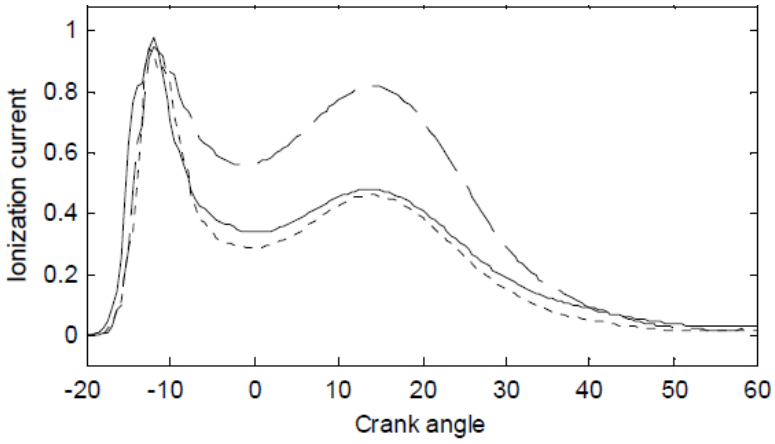

Figure 1.12: Fuel Properties Affect on Ion Current. RON 98 (solid), Leaded Fuel (dash), Propane (dot) [6]

The engine under observation in Kubach et al. [2] had an intake port deactivation system which allowed them to study the effects of swirl on ion current. At 1500 RPM and 4 bar BMEP, the engine was run with the charging port opened and closed. In this configuration, the swirl ratio was the highest with the charging port closed. In *Figure 1.13,* the authors showed that whether or not the valve was open was detectable with ionization. Interestingly, the main ion current peak increased in amplitude under the high swirl condition, while the minor peaks decreased when compared to the low swirl state.

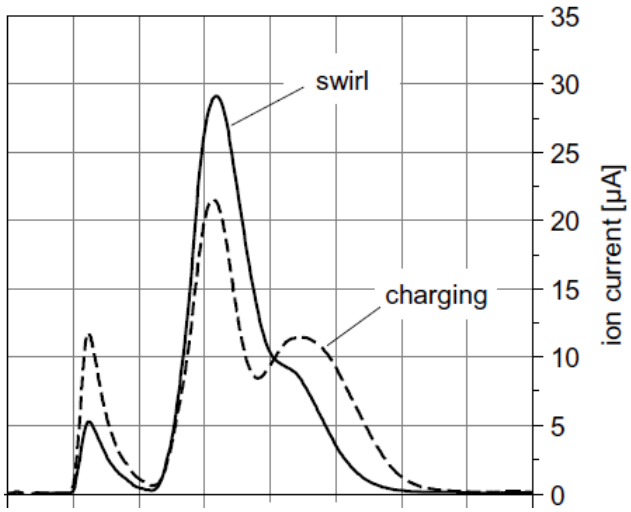

Figure 1.13: Effect of Swirl Ratio on Ion Current Signal [2]

In addition, they investigated the effects of EGR and pilot injection. Pilot injection decreased the amplitude of the ion current with or without EGR. Therefore, the occurrence of a pilot injection is detectable. In addition, the authors suggested that the pilot quantity could indirectly be measured by the correlating the ignition delay from the ion current signal to the injected quantity. *Figure 1.14* and *1.15* shows the impact of pilot injection and EGR.

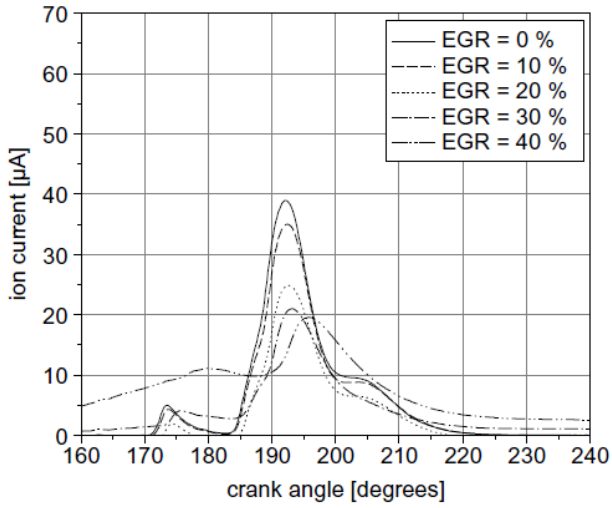

Figure 1.14: EGR Sweep Without Pilot Injection [2]

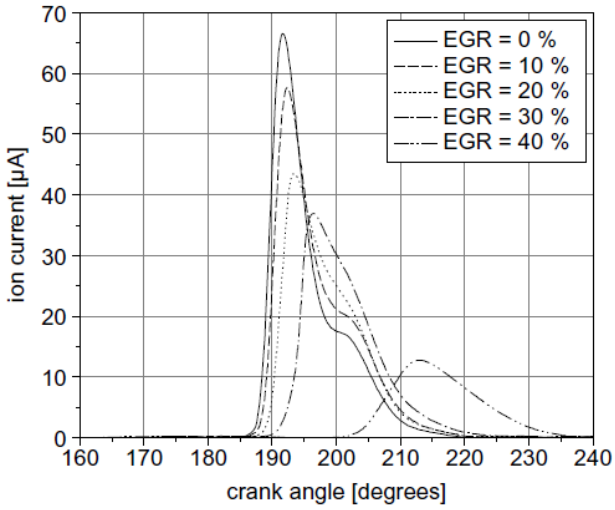

Figure 1.15: EGR Sweep with Pilot Injection [2]

For EGR, not only was the presence of EGR detectable, but the authors claimed the level of EGR could be determined as well. In order to do this, the ion current signal offset was set to zero at SOC. Correlation coefficients were very high between ion current and EGR percentage as is seen in *Figure 1.16.*

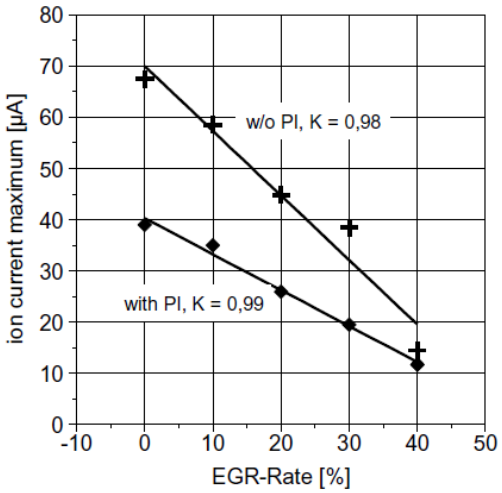

Figure 1.16: Correlation of EGR Percentage to Ion Current Amplitude [2]

Lastly, the authors investigated the start of combustion (SOC) measured by cylinder pressure and ion current measurements. The local minimum before the start of main combustion was used to set a threshold value for SOC. Steady-state testing at 1500 RPM and 8 bar BMEP revealed two things. First, an offset between SOC determined by the burn rate, ion current, and the derivative of the ion current was discovered. The authors noted that this offset which ranged from 1-3 CAD could only be experimentally determined as it would change throughout the operating map. *Figure 1.17* displays the offset between the different methods of determining SOC.

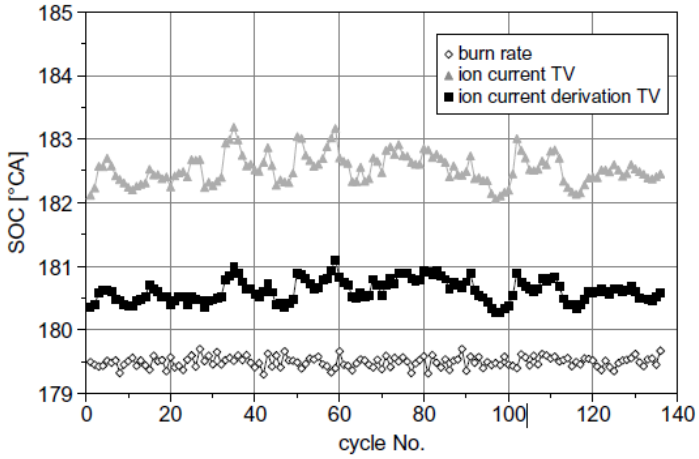

Figure 1.17: Offset Between the Different Methods of Finding SOC [2]

The authors also compared the standard deviation between the burn rate, ion current, and the derivative of ion current. The data collected from approximately 140 engine cycles. In *Figure 1.18*, ion current is shown to have the largest degree of deviation at about 0.23 CAD.

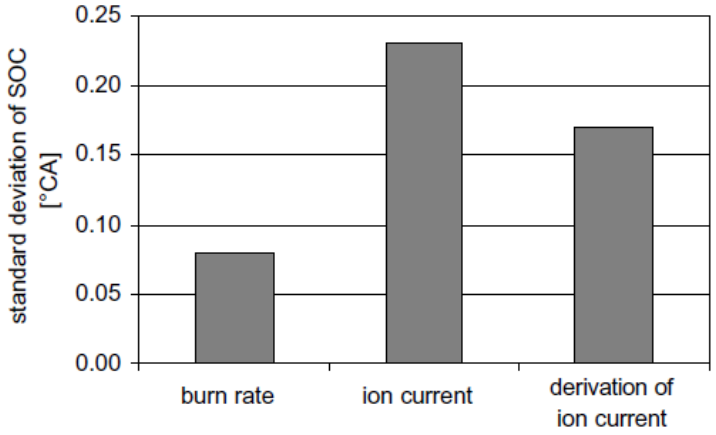

Figure 1.18: Comparison of Standard Deviation [2]

In addition to their steady-state testing, the authors also compared transient operating conditions which are more relevant for real engine cycles. IMEP was varied at a constant engine speed of 1500 RPM. The transient change of SOC is plotted in *Figure 1.19.*

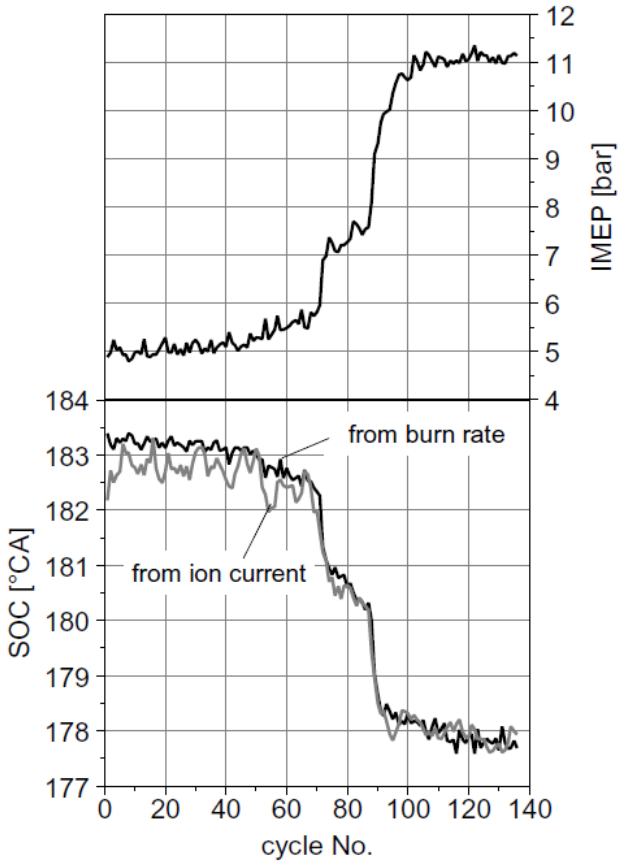

Figure 1.19: Transient Comparison Between Burn Rate and Ion Current in Determining SOC [2]

In Henein et al. [9], a comparison between experimental results of SI, HCCI, and CI ion current measurements is made. For CI engines, the authors divide the ion current trace intro four peaks and offer explanations for each. It is to be noted that all four peaks are not present at all times. There is a dependence on engine operating conditions between the number and size of the ion current peaks. Experiments were performed on a single-cylinder engine. An example of the ion current peaks is given in *Figure 1.20*.

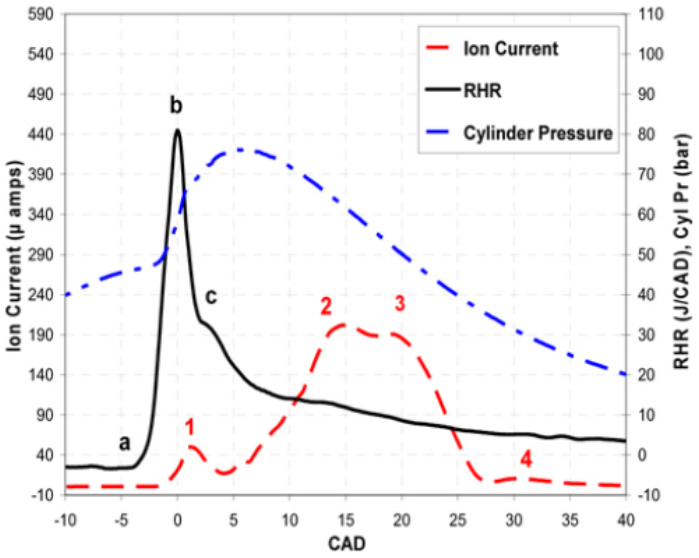

Figure 1.20: Example of Four Ion Peaks in Diesel Engine [9]

Regarding the first ion current peak, several observations are made by the authors. First, there is a delay of approximately one CAD between the peak in RHR (rate of heat release) and Peak 1. The RHR is calculated from the in-cylinder pressure measurement. This measurement is a global characteristic of the cylinder. Unlike the pressure transducer, the ion current probe is sensitive to the location in the combustion chamber. The farther the probe is from the first-in-line spray, the longer the delay between the RHR and Peak 1. Also, the authors suggest that the response of the electronic circuits could be contributing factor in the delay. However, the electronic circuits used in the amplification and processing of the pressure transducer and ion current probe should be of the same order.

Another important characteristic regarding Peak 1 is the process responsible for its formation. In-cylinder temperatures at the beginning of combustion are much lower than those at the end. Because of this, the authors determined it was not thermal ionization, but chemi-ionization responsible for the first ion current peak.

Lastly, the authors attribute Peak 1 to the premixed combustion of the main injection. In their experimental setup, no pilot injection was used. However, the authors admitted that if a pilot injection had been used as was done in Kessler [16] and Kubach et al. [2], there probably would have been an ion current peak due to the pilot injection before Peak 1.

Peak 2 was determined to be caused by the turbulent premixed and diffusion flames of the second-in-line spray. Based on the phase shift between Peak 1 and Peak 2, the amount of time, 2.3ms, between the two peaks was calculated. In order for the second-in-line spray to be the cause of Peak 2, it would have to reach the ion probe in 2.3ms. For the given engine speed, the swirl ratio was estimated to 4.35. Since this is a reasonable estimate for swirl ratio, it was concluded that Peak 2 was caused by the second-in-line spray.

Peak 3 was too close to Peak 2 to be caused by the third-in-line spray. The authors suggest that Peak 3 is caused by the reflection of the second-in-line spray off of the surface of the combustion chamber walls.

Lastly, Peak 4 exhibits low amplitude due to the drop of combustion temperature. The same method for estimating the swirl ratio between Peak 1 and Peak 2 was applied between Peak 3 and Peak 4. However, the authors were not confident that Peak 4 was a result of the third-in-line spray because the estimate of the swirl ratio resulted in an 11% loss of motion. Also, Peak 4 was only measureable at high loads when there is enough time for the combustion products to burn and reach the ion probe.

In this same paper, the authors also studied the impact of engine load on ion current as represented in *Figure 1.21.* As load increased, the amplitude and information from ion current peak increased as well. This is because at higher loads more fuel is injected into the cylinder. In addition, the fuel is injected over a longer period of time. These two factors increase the premixed and diffusion combustion.

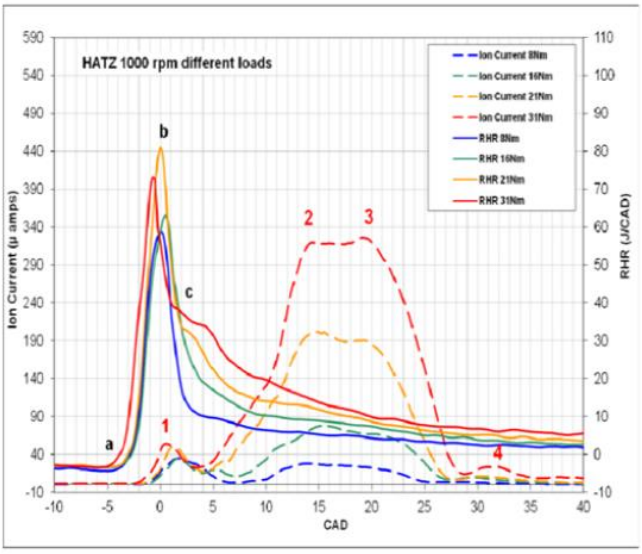

Figure 1.21: Increase in Ion Current Due to Engine Load [9]

Estefanous et al. [5], introduce a new type of ion probe, the fuel injector. An injector was energized with a positive 100V DC. The author was able to demonstrate an advantage to this type of probe. Based on the ion current signal, injector malfunctions such as leakage or fluctuations in needle lift were able to be detected. In addition, an overlay of injector current and ion current were made. The author was able to show that the energizing and de-energizing of the fuel injector was detectable by the ion current. *Figure 1.22* displays a successful injection versus a malfunction.

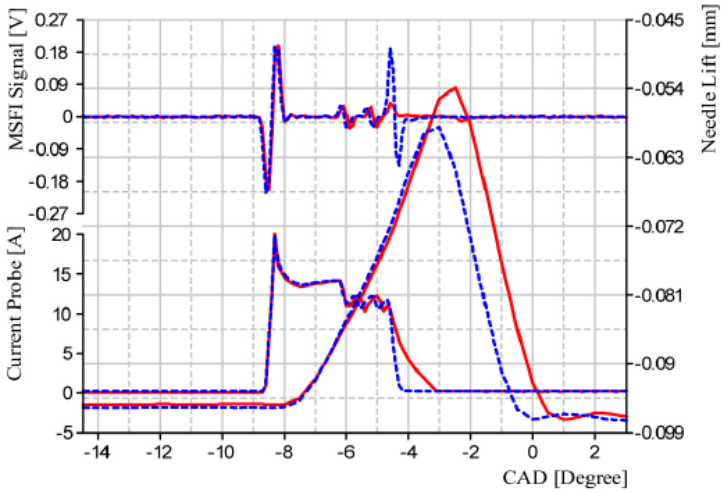

Figure 1.22: Multi-Sensing Fuel Injector Signal Compared Over a Successful Injection (blue) and Faulty Injection (red) [5]

The author also presented a simulation that compared the sensitivity to location of the fuel injector to a glow plug. This was done by placing a charged particle on each side of the combustion bowl. The central location of the fuel injector allowed it to sense the charged particle on either side of the bowl. However, the glow plug could not sense the charged particle when it was on the opposite side due to the long distance. *Figure 1.23* shows a representation of the simulation results.

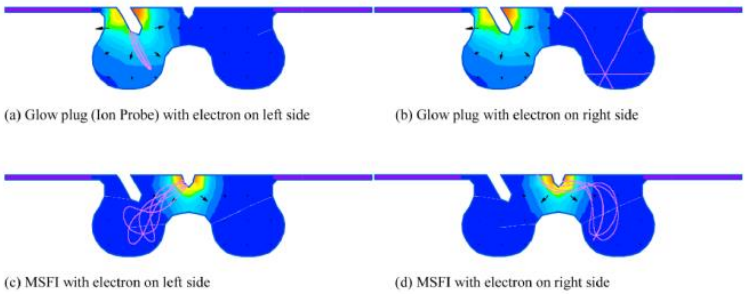

Figure 1.23: Simulation of Ion Probe Sensitivity to Location [5]

In Badawy et al. [3], the authors investigated four features of the ion current to determine which could best be related to a combustion phasing parameter. These features included start of ion current (SIC), first peak of the derivative of ion current (i'_1), first ion current peak (i_1), and second ion current peak (i_2). Examples of ion current features are given in *Figure 1.24.*

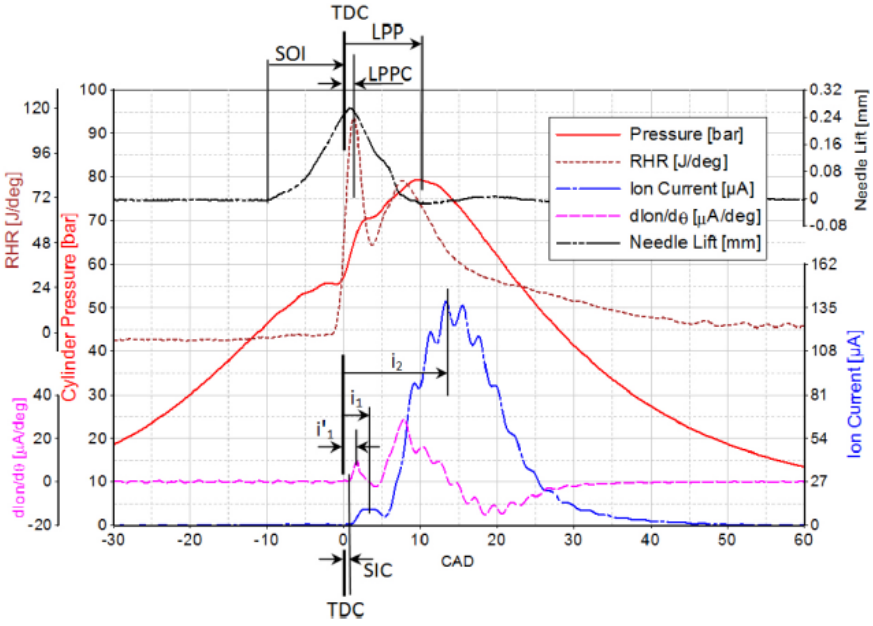

Figure 1.24: *Examples of Ion Current Features Studied for Correlation to Combustion Phasing [3]*

Under steady-state conditions, SIC had the lowest amount of variation over the other ion current features. The next step was to determine whether or not a correlation between SIC and LPPC (location of the peak of the RHR due to premixed combustion) could be made. This was accomplished by doing two different parameter sweeps. First, with SOI held constant, a sweep of fuel injection pressures and engine load was performed. As shown in *Figure 1.25*, the agreement between LPPC and SIC was very tight. However, an offset of 0.45 CAD of SIC from LPPC was noticed.

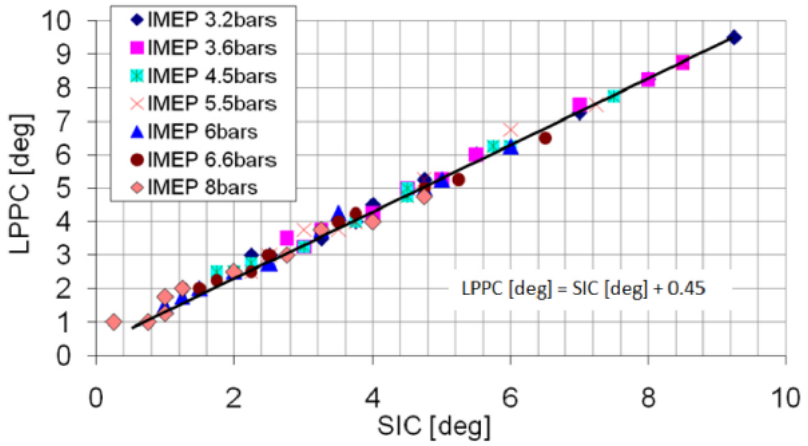

Figure 1.25: *Relation of SIC to LPPC Under Constant SOI with Variable Load and Injection Pressure [3]*

A second test was performed under which injection pressure was held constant, but engine load and SOI timing was varied. Again, good agreement between SIC and LPPC was found. However, the offset went down from 0.45 CAD on the previous test to 0.35 CAD. *Figure 1.26* represents the relationship between SIC and LPPC under these engine operating conditions.

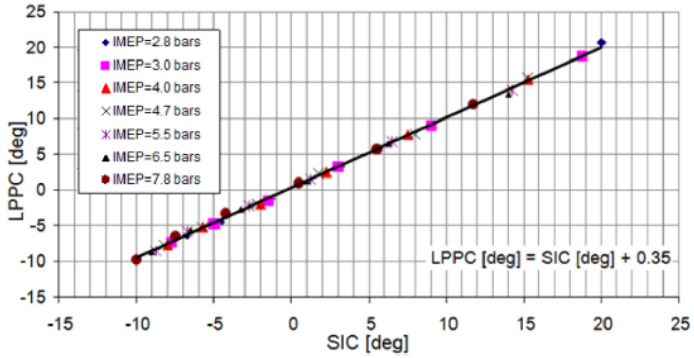

Figure 1.26: Relation of SIC to LPPC Under Constant Injection Pressure with Variable Load and SOI Timing [3]

To demonstrate ion sensing under closed-loop engine control, the authors developed an algorithm and implemented it in an open ECU. Before switching to closed-loop control, a set of steady-state measurements of SIC and LPPC were taken to determine the variation of each parameter. This was done to make a comparison between open-loop and closed-loop control. *Figure 1.27* shows the results of open-loop control and *Figure 1.28* shows the results of closed-loop control.

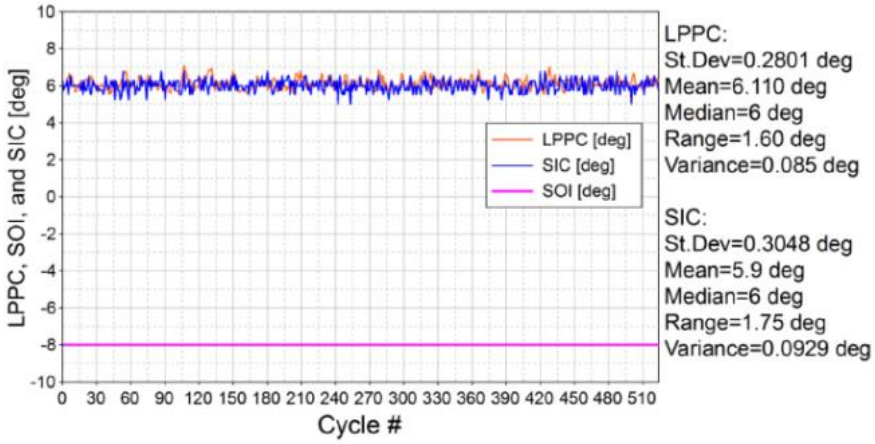

Figure 1.27: Variation of SIC and LPPC Under Open-Loop Control [3]

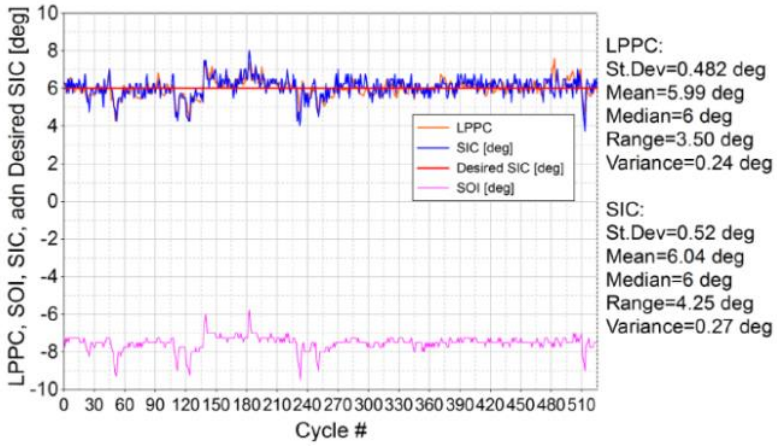

Figure 1.28: Variation of SIC and LPPC Under Closed-Loop Control [3]

As can be seen from the *Figure 1.27* and *1.28*, open-loop control still had less variation than closed-loop control using ion sensing. The authors were also able to demonstrate closed-loop control over a transient period in addition to the steady-state period shown in *Figure 1.28.* However, no comparison was made over open-loop control for the same transient period.

In this paper, Badawy et al. [17] used ionization as a means of estimating soot formation. Results from a non-linear multiple regression (NLMR) model were compared to the instantaneous measurements from a opacity meter. Initially, the sensitivity of the number of inputs in the NLMR was studied. It was proven that as the number of inputs increase, the model's effectiveness improved by the decrease in mean square error and increase in determination. Several transient tests were run and the opacity meter's measured soot was compared to the NLMR model's estimated soot. The first transient condition held engine speed steady at 1800 RPM while varying engine load and fuel injection pressure. The measured soot and estimated soot correlated tightly as seen in *Figure 1.29.*

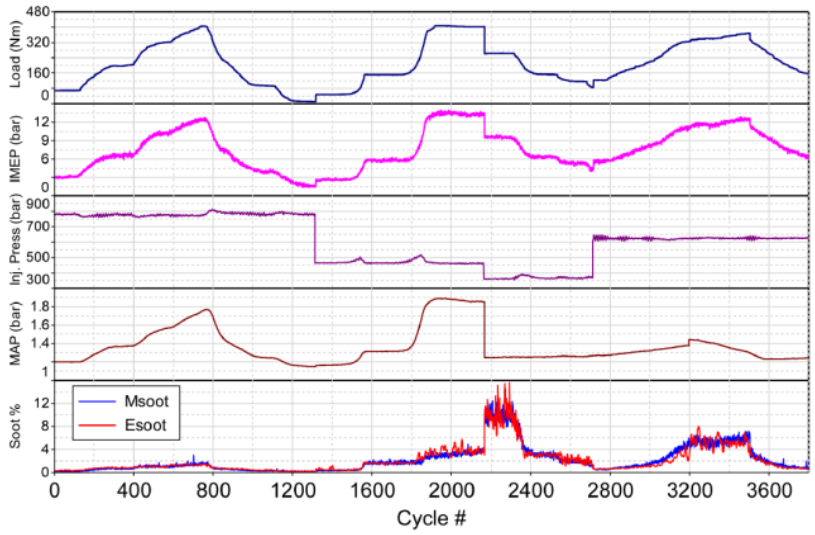

Figure 1.29: Comparison of Measured and Estimated Soot with Varied Load and Injection Pressure. [17]

In the next transient test, the engine speed was changed from 1000 to 2000 RPM while holding engine load constant. Fairly good agreement was witnessed between the measured soot and estimated soot. *Figure 1.30* shows the results of their testing. The authors attributed the discrepancy between measured soot and estimated soot on intervals of cycle 100-130 and cycle 360-390 to a limitation of the response of the opacity meter.

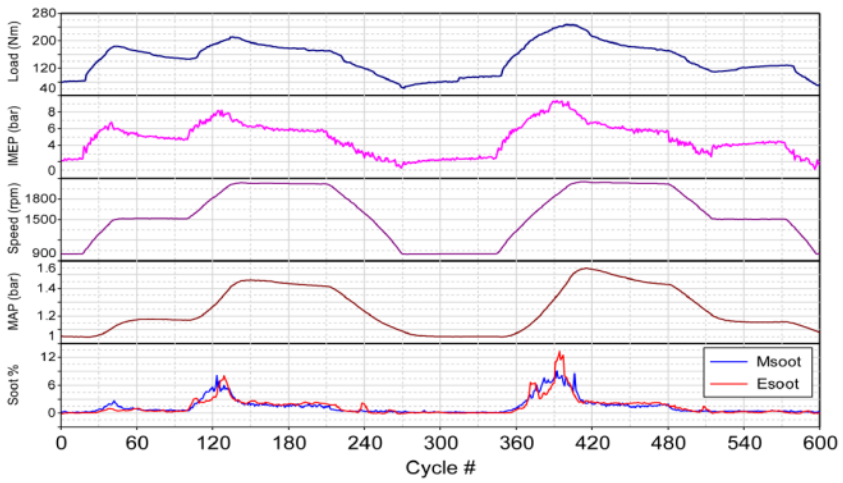

Figure 1.30: Comparison of Measured and Estimated Soot Under Constant Engine Load with Varied Engine Speed [17]

Lastly, a final transient test was performed where engine speed and load were held constant while manifold absolute pressure varied from 1.15 to 1.27 bar. *Figure 1.31* displays the test results. The measured soot and estimated soot did not agree as well as in the previously transient tests. The authors attributed this to the low amount of soot to be measured and the response time of their opacity meter.

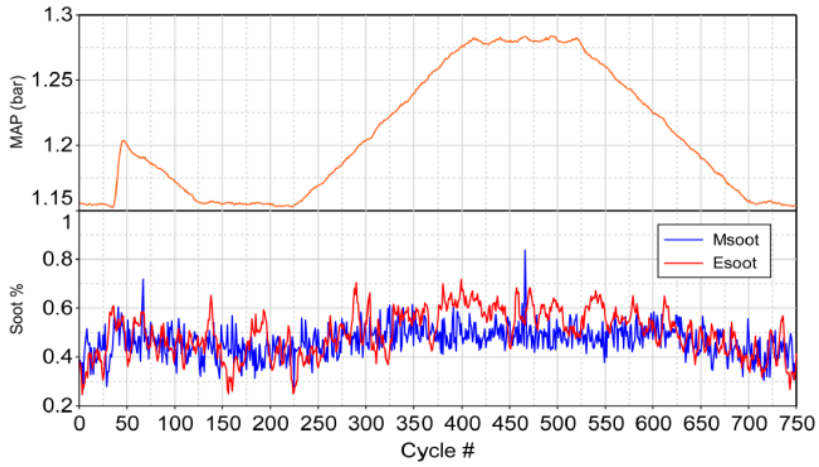

Figure 1.31: Comparison of Measured and Estimated Soot Under Constant Engine Speed and Load with Varied MAP [17]

Estefanous et al. [10] modified a NO sampling probe for the purpose of measuring ion current. This allowed the researchers to monitor in-cylinder NO and ionization at the same time. In addition, a model was proposed for estimating the contribution of NO to thermal ionization. From using this model, it was found that the contribution of NO concentration on thermal ionization was insignificant when compared to raising in-cylinder temperature. However, ion current increased dramatically when the mass

average temperature was doubled, but barely increased when NO concentration was raised ten times. Based on these calculations, the authors believe that thermal ionization does not contribute in a significant way until the mass average temperature is above 2000 K. The authors also took many measurements at injection pressures of both 400 and 1000 bar while varying IMEP. While some similarities existed between the profiles of NO concentration and ion current, no correlation can be easily drawn and none was suggested by the authors. *Figure 1.32* shows an example of the comparison of ion current to NO measurements at three different cycles for the same engine conditions of 1000 bar injection pressure and 11 bar IMEP.

In Henein et al. [6], several different parameter studies were carried out to understand the effect of engine load and injection pressure on ion current. Holding engine speed and load constant, injection pressure was varied from 400 to 850 bar. *Figure 1.33* shows the results.

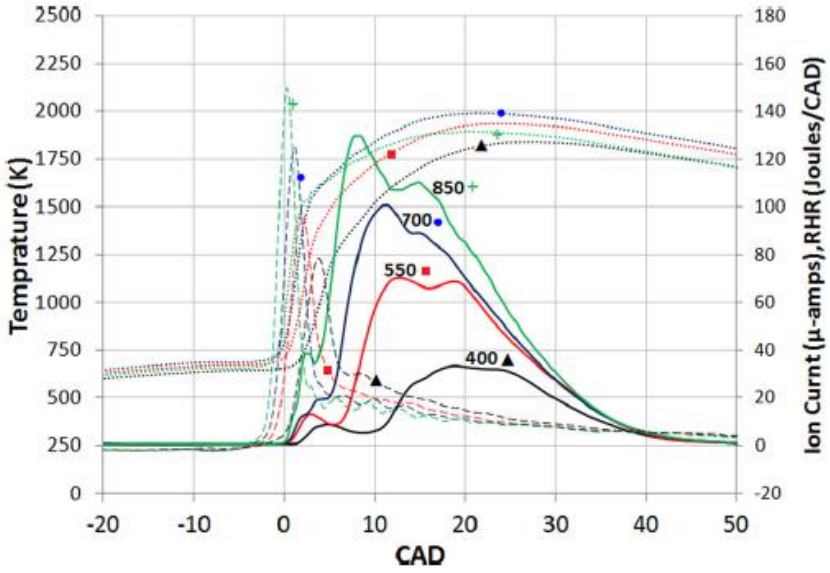

Figure 1.32: Comparison of Ion Current with Varied Injection Pressure [6]

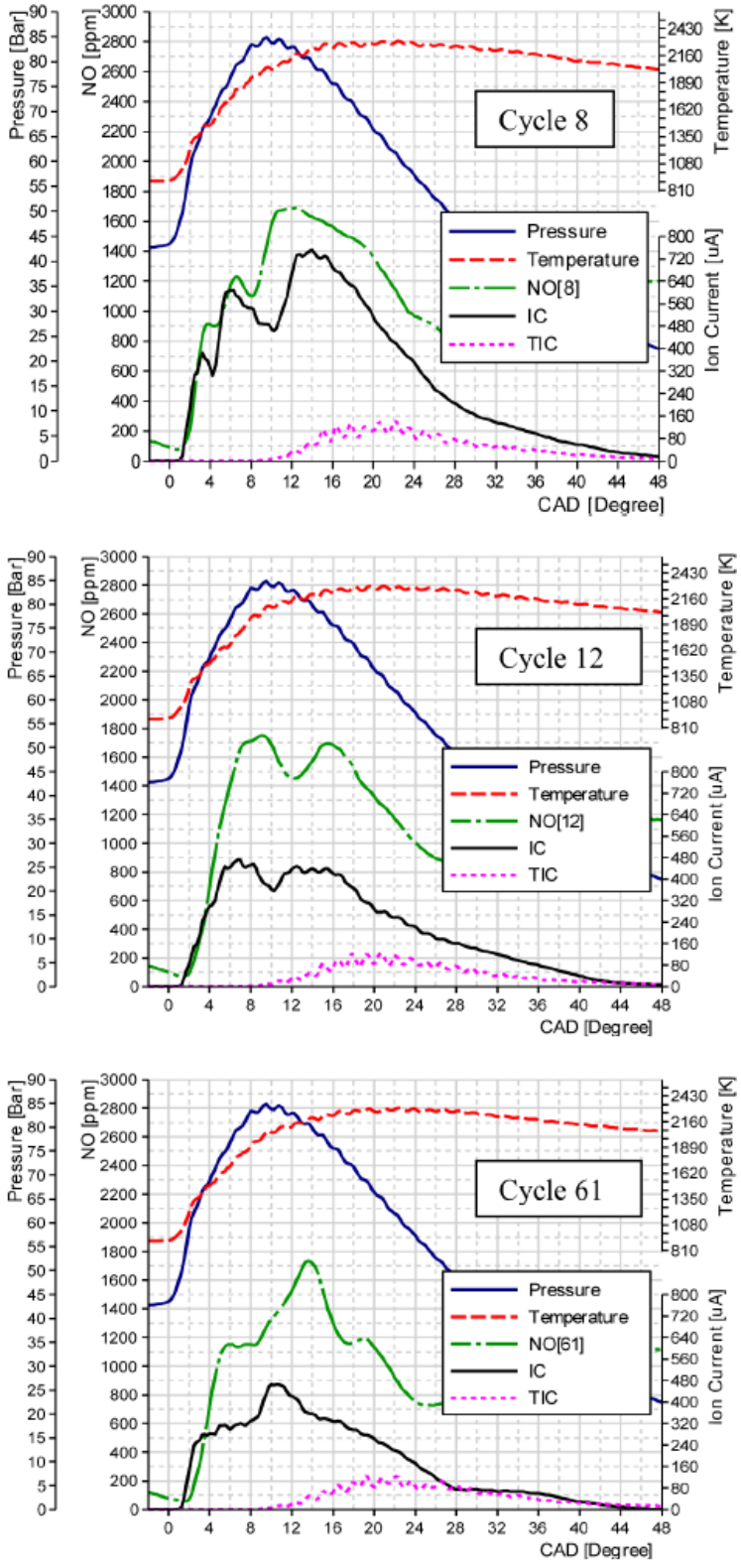

Figure 1.33: Ion Current Compared to NO at Cycle 8, 12, and 61 [10]

The authors explained that increasing injection pressure increased the first peak of ion current, I_1, due to the larger premixed fraction of the first spray to reach the ion current probe. The increase in premixed fraction along with the rise in local gas temperatures enhanced and accelerated the chemical reaction responsible for producing ion current in both the chemi-ionization and thermal ionization.

Next, the effect of engine load on ion current was studied by holding engine speed constant at 1800 RPM and injection pressure at 850 bar while varying IMEP from 5 to 11 bar. In general, ion current increased with load. This is not surprising since the increase in load causes an increase in both the mass of fuel injected into the cylinder and the increase in the duration of the injection. The relationship of engine load to ion current is shown in *Figure 1.34.*

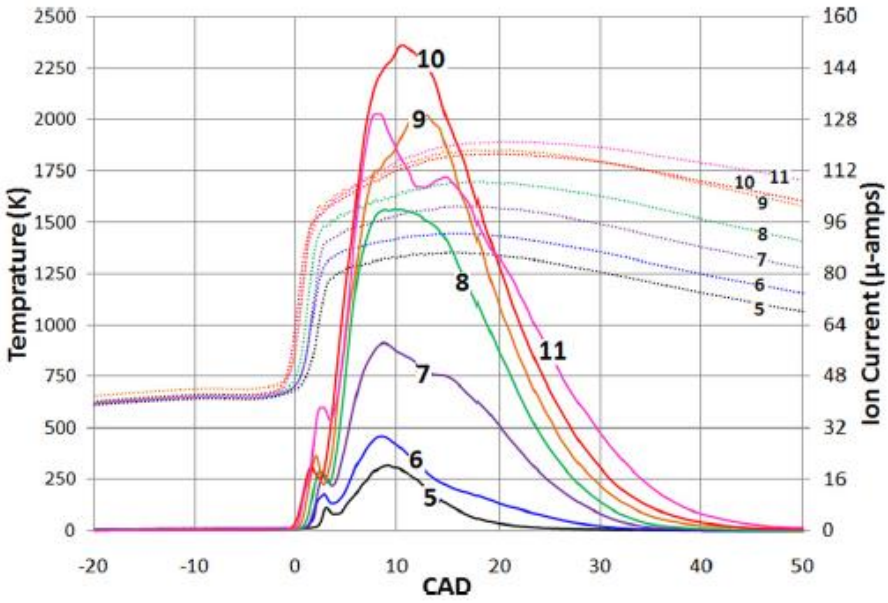

Figure 1.34: *Relationship of Ion Current to Engine Load [6]*

Lastly, all of their test points were summarized in a single plot where max ion current was correlated to NO and soot emissions in *Figure 1.35*. IMEP was varied from 5 to 11 bar and is labeled on the plot in parentheses. Injection pressure was varied from 250 to 850 bar and is labeled in brackets. Opacity is represented with a dashed line while soot is represented with a solid line.

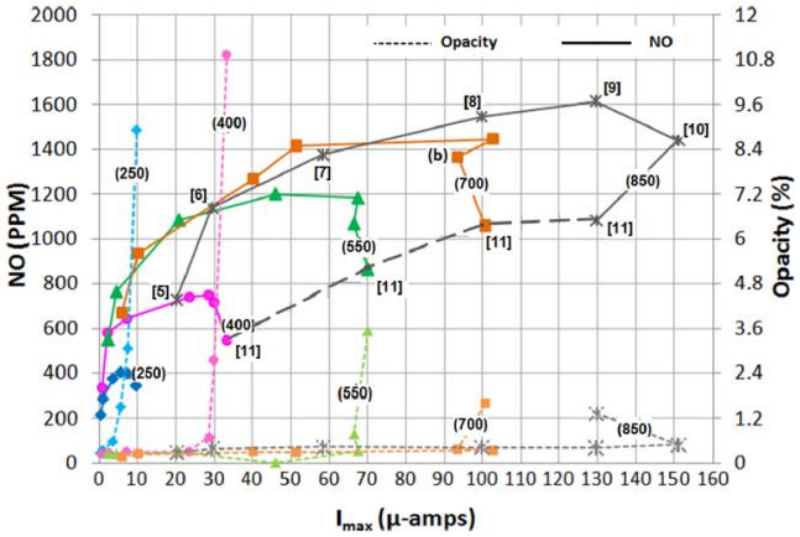

Figure 1.35: *Correlation of Max Ion Current to NO and Soot Emissions [6]*

1.4 CONCLUSION

From this review of ion current literature, it has been shown that ion current is a capable in-cylinder sensor for measuring multiple engine operating parameters. However, implementation and real-world gains in passenger car and heavy-duty diesel engines is still challenging due to variability of the ion current signal. This requires the ECU to store large amounts of high frequency data, average and filter the results, and make engine calibration changes in real time. The processing power required to do these tasks is at the limit of most ECUs. In the future, ionization may prove to be a valuable resource in reducing fuel economy and engine emissions as technology increases.

CHAPTER 2.0 : MODERN FUEL INJECTION EQUIPMENT

2.1 HYDRAULIC-ELECTRONIC UNIT INJECTION

The origin of hydraulic-electronic unit injection (HEUI) began in the 1990s. In an agreement between Caterpillar and Navistar, Caterpillar developed the HEUI system [18]. HEUI stands superior to every preceding version of unit injection because of its freedom from mechanical actuation. Injection events are independent of camshaft position giving flexibility to engine timing. In the following section, a brief description of the Caterpillar HEUI system is given. This is followed by a detailed explanation of the fuel injector and fuel pump. Lastly, a summary of the advantages and disadvantages of the HEUI system is provided.

The major components to the HEUI system include the hydraulic unit injector pump, unit injector, engine control module (ECM), fuel transfer pump, and injection actuation pressure sensor. A system diagram is provided in *Figure 2.1*.

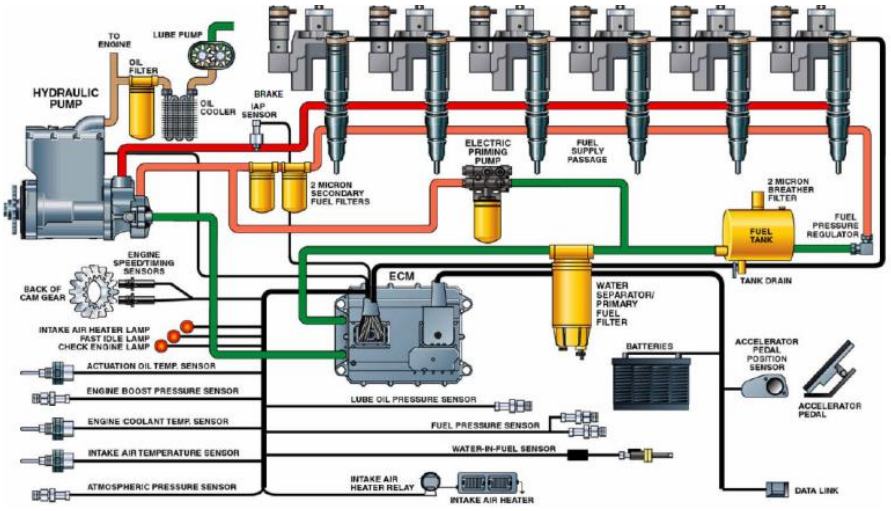

Figure 2.1: Caterpillar HEUI System Diagram [19]

The journey of the fuel from the fuel tank to the combustion chamber begins with the fuel transfer pump. This pump lifts fuel from the tank and sends it to the unit injectors via a single passage in the cylinder head. This passage feeds all of the unit injectors. Fuel enters the unit injector at a very low pressure. In order to pressurize the fuel, high pressure oil is delivered to the unit injector through passages in the cylinder head by the hydraulic unit injector pump. The oil that supplies the hydraulic unit injector

pump is taken from the engine lubrication oil system. A solenoid within the unit injector controls the oil flow based on signals from the ECM. Also inside the unit injector, an intensifier piston is activated by the high pressure oil. The intensifier piston multiplies the pressure of the oil compressing the fuel in the unit injector to a very high pressure, approximately six times the pressure of the oil [20]. During the fuel injection process, the ECM receives feedback from the injection actuation pressure sensor. This measures high pressure oil at the oil rail providing closed-loop control over the oil circuit. The ECM reads the pressure signal from the injection actuation pressure sensor and adjusts the pressure regulator in the hydraulic unit injector pump accordingly.

Figure 2.2 displays the physical appearance of the HEUI injector. Within the fuel injector itself, there are many processes and components that control each injection event. *Figure 2.3* provides an illustration of each part and their name.

Figure 2.2: *HEUI Fuel Injector*

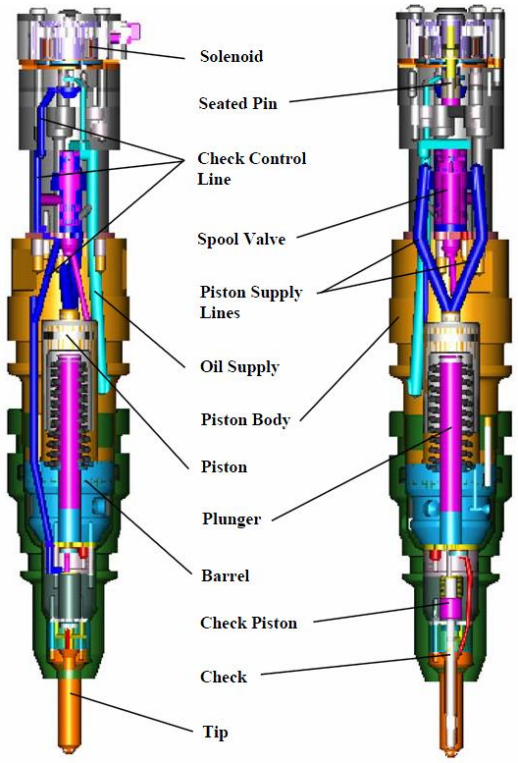

Figure 2.3: *Caterpillar HEUI fuel injector [19]*

In understanding the HEUI injector, it is important to distinguish between the high pressure actuation oil circuit and fuel supply circuit. In a sense, the behavior of the actuation oil circuit and fuel supply circuit can be described as a master/slave relationship with actuation oil being the master. It is the actuation oil that determines the injection timing, duration, rate shape, and pressure.

The flow of high pressure oil from the hydraulic unit injector pump into the injector begins when the ECU energizes the solenoid inside the fuel injector. This solenoid controls the position of the seated pin. The seated pin has two needle seats, upper and lower, which allow it to perform two main functions. First, when the solenoid is energized, the seated pin is against its upper seat. This allows oil to drain out of the check control line and from under the spool valve. Relieving oil pressure in the check control line permits the nozzle to open when high pressure fuel is present. Simultaneously, actuation oil begins to flow past the spool valve while the seated pin is in the upper position. Once past the spool valve, the actuation oil reaches the intensifier piston. The actuation oil forces the intensifier piston downward

compressing the fuel to 180 Mpa. Once the fuel reaches a pressure greater than the force of the nozzle spring, the nozzle opens and fuel injection begins.

The second main function of the seated pin occurs when the solenoid is de-energized and the pin is on its lower seat. In this position, actuation oil flows down the check control line to the check piston. The check piston is responsible for closing the nozzle at the end of injection. As the check piston closes the nozzle, actuation oil flows under the spool valve closing the flow to the intensifier piston.

The fundamental principle that allows the HEUI injector to rate shape is the speed at which the spool valve and solenoid operate [19]. The solenoid can actuate at a much higher rate than the spool valve. Therefore, the solenoid is able to open, partially pressure the fuel, and close without the spool valve moving. With high pressure fuel primed in the injector tip, the solenoid is energized and high pressure fuel is instantly available when the nozzle opens. By manipulating the solenoid current, a variety of schemes can be generated. For further explanation, more details are provided in [19]. *Figure 2.4* shows the injector fill scheme to produce a square rate shape [NOTE: Orange=High Pressure oil, Green=Empty Oil Passage, Red=High Pressure Fuel].

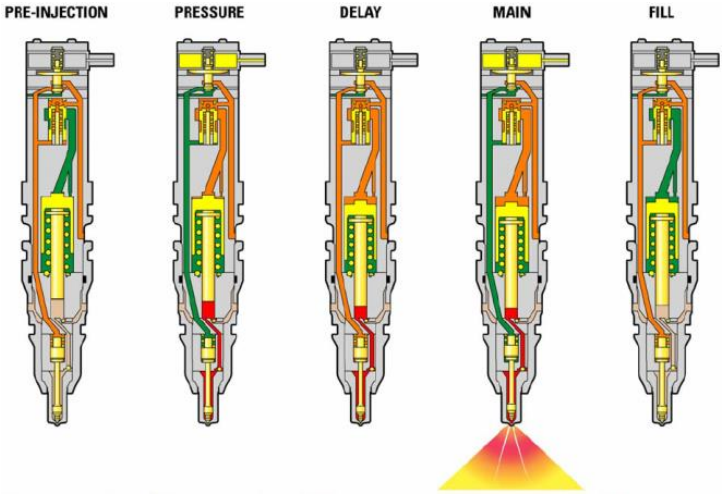

Figure 2.4: Fill Scheme for Square Rate Shape [19]

In the HEUI system, there is a high pressure oil pump (unit injector hydraulic pump) and a low pressure fuel pump that supply their respective fluids to the unit injector. Although mounted on the back side of the high pressure oil pump, the fuel pump is a separate pump entirely. The fuel pump is driven by

a shaft from the high pressure oil pump. The fuel pump is responsible for transferring fuel to the injectors at a low pressure of 450 kPa [20].

The high pressure oil pump is a variable delivery piston pump. It is gear driven off of the front gear train of the engine. Based on commands from the ECU, the high pressure oil pump provides oil to the unit injectors at a pressure of 6 Mpa to 28 Mpa [20]. Although the engine has a dedicated lubrication oil pump, oil is shared between the lubrication oil pump and the high pressure oil pump.

The HEUI system offers several advantages that make it suited for modern diesel engines. First, the unit injector is not mechanically driven by the engine. This allows for flexibility in injection timing, duration, and number of injections. Second, HEUI delivers injection pressures of 180 Mpa. High injection pressure has many emissions and engine performance benefits. Lastly, HEUI provides control of the injection rate shape. Ramp, boot, and square injection rate profiles are fully obtainable.

Unfortunately, all of these benefits introduce a high system complexity. To create the fuel and oil rails, the cylinder head machining is increased. In addition, the unit injector itself has many intricate moving parts. Another detriment occurs when leakage between the oil and fuel passages in the injector takes place. Lastly, the injection events do exhibit variability from fluctuations in oil temperature and other factors.

2.2 HIGH-PRESSURE COMMON RAIL

High-pressure common rail (HPCR) fuel injection is newer then the HEUI system and has been widely accepted in the heavy duty diesel market. Like HEUI, HPCR injection events are independent of camshaft position giving flexibility to engine timing. Although most HPCR systems share many similarities, one common difference is the fuel injector type: solenoid or piezoelectric. Piezoelectric is often preferred in HPCR systems because of its faster response time over solenoid actuated injectors. This allows for higher precision in injected fuel quantity and fuel injection timing. It also enhances the capability for multiple injections. For these reasons, the HPCR system described in this paper incorporates the piezoelectric fuel injector type. In the following section, a brief description of the Bosch

CRI3 HPCR system is given. This is followed by a detailed explanation of the fuel injector and fuel pump. Lastly, a summary of the advantages and disadvantages of the HPCR system is provided.

The major components for HPCR are high pressure fuel pump, pressure control valve, fuel rail, rail pressure sensor, fuel injector, and ECM. A system diagram is provided in *Figure 2.5*.

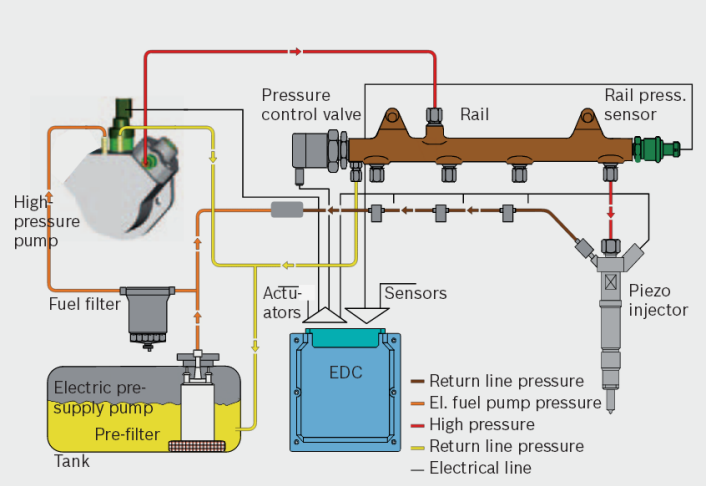

Figure 2.5: *Bosch CRI3 System Overview [21]*

Diesel fuel is lifted from the storage tank by a low pressure fuel pump. After passing through a filter, the fuel is delivered to the high pressure fuel pump. The high pressure pump compresses the fuel to 180-200 Mpa [22]. The fuel leaves the high pressure pump through high pressure fuel lines and enters the fuel rail. At the rail, fuel is distributed to the fuel injectors. The ECM controls the opening and closing of the fuel injector. In addition, the ECM receives feedback from the rail pressure sensor and transmits signals to the pressure control valve and high pressure pump to maintain the desired fuel pressure.

Figure 2.6 displays the physical appearance of the Bosch CRI3 piezoelectric fuel injector while *Figure 2.7* depicts the inner workings.

Figure 2.6: *Bosch CRI3 fuel injector [21]*

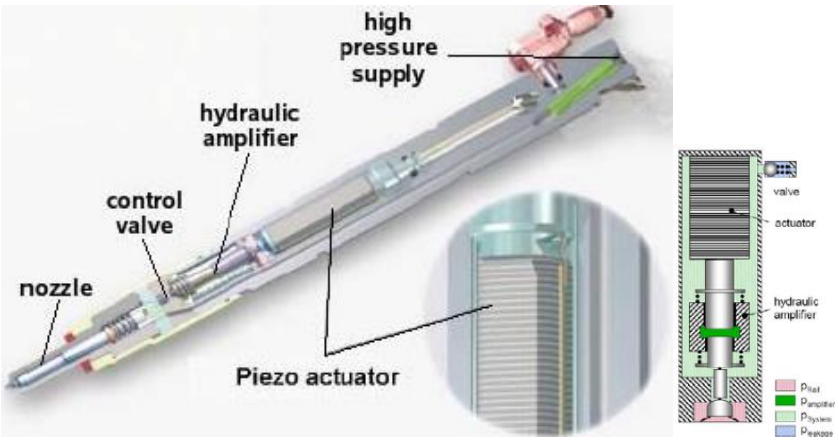

Figure 2.7: *Bosch CRI3 internal components [22]*

At the heart of the CRI3 fuel injector is the piezoelectric stack. The piezo stack is a dense grouping of ceramic layers. These layers are connected electrically in parallel. When they are energized, the resultant electric field produces a mechanical strain which causes the stack to expand 40-50 μm [22]. The piezo stack does not operate the control valve directly, but requires a hydraulic amplifier. The hydraulic amplifier is needed to multiply the precise motion of the piezo stack to that which is necessary to move the control valve.

The control valve manages the flow of fuel through the injector. *Figure 2.8* shows the control valve in its three positions: starting; needle opening; and needle closing.

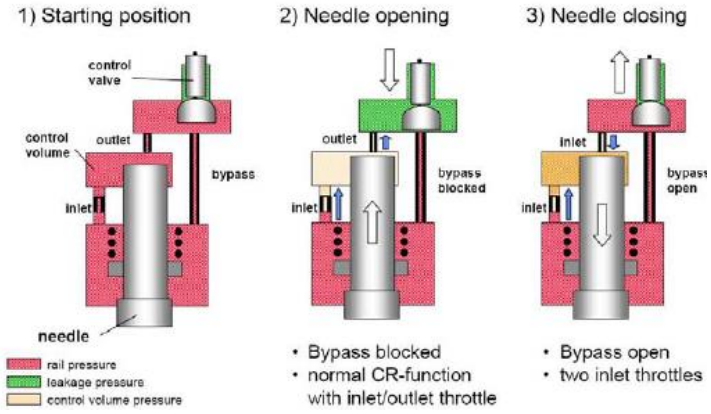

Figure 2.8: *Control Valve Positions [22]*

In the starting position, the control valve and fuel injector needle are both closed. In the control volume and bypass passage, fuel is pressurized to the rail pressure. High pressure fuel in the control volume forces the needle downward keeping the injector closed. Once the piezo stack is energized, the

control valve moves to the open position. Here, the bypass passage is blocked and fuel drains from the control volume through the outlet passage. As the control volume drains, the pressure above the needle is reduced allowing it to open. To end an injection event, the piezo stack is de-energized. Subsequently, the control valve shuts which opens the bypass passage. The high pressure fuel fills the control volume which in turn closes the needle.

In a piezoelectric fuel injector, the mechanics of injection rate shaping are much simpler than the HEUI system because its ability to create rate shapes is much more limited. Rate shapes are produced by partially lifting the needle. With the needle valve partly opens, fuel flow is throttled to the nozzle holes [23]. Although this does produce some limited rate shaping, deterioration of the spray pattern occurs hindering engine performance.

The Bosch CP3 fuel injection pump is a gear-driven radial piston pump [23]. Inside the pump, there is both a low pressure and high pressure fuel circuit. The low pressure circuit delivers fuel to the high pressure circuit. The amount of fuel transferred to the high pressure circuit is controlled through a pressure regulator. Excess fuel is used to cool the pump and bled back into the pump inlet [23].

In the high pressure circuit, fuel enters the pump's three cylinders. Here, it is pressurized by plungers to the rail pressure [23].

The advantages of the HPCR system are similar to the HEUI. HPCR offers flexible injection timing because the injector is not mechanically constrained to engine speed or timing. In addition, HPCR offers high injection pressure of 180-200 Mpa. Lastly, injection rate shaping is possible through needle throttling.

One of the disadvantages of the HPCR with piezoelectric injectors is the added cost due to the piezo stack. Another disadvantage is the needle throttling necessary to perform injection rate shapes. Lastly, HPCR systems typically are not able to conform their injection rate to the boot rate shape and their control over the slope of ramp rate shape is limited.

2.3 MAJOR VARIABLES OF THE MODERN FUEL INJECTION SYSTEM

In order to control emissions, reduce fuel consumption, and increase specific power output, fuel injection systems of the modern diesel engines have many variables to control. The major parameters to control are the injection pressure, injection timing, duration of injection, number of injections, and injection rate shape. In the next section, a description of the impact of each of these elements is provided. Also, a brief literature review is given to support the influence of these elements. For the purpose of this paper, such things as injector hole diameter, number of spray holes spray angle, injector nozzle type, etc. are viewed as properties of the fuel injector itself. These properties are omitted from the following discussion as they do not pertain to the fuel injection system as a whole. In addition, injection timing and duration will not be covered since varying these parameters is not unique to modern fuel injection systems.

2.3.1 Injection Pressure

Injection pressure of the typical modern fuel injection system ranges from 180 Mpa (1800 bar) to 300 Mpa (3000 bar). Recent improvement in fuel injector nozzle design and manufacturing processes promise even higher injection pressures. High fuel injection pressure is a proven method for decreasing harmful exhaust emissions [24, 25, 26]. In addition, it is the preferred method for increasing fuel flow rate when raising power density [27].

Fischer et al. [24] determined there is a critical limit to the benefit of increasing injection pressure. In their study, the pressure of a single main injection from a 200 Mpa (2000 bar) HPCR system was varied. Simultaneous soot-Nox emission reduction was achievable until reaching a critical limit where further pressure increases yielded no additional benefit. Boot pressure, engine load, and start of injection were the main factors in defining the critical injection pressure limit.

Abdullah et al. [25] found high fuel injection pressure is a means of reducing HCs, smoke, and CO. However, this caused a rise in Nox. Using EGR with high fuel pressure and split injections can

together lower both Nox and other harmful emissions. In this paper, a series of experiments were run with fuel injection pressures ranging from 300-700 bar. EGR, engine speed, and engine load were varied to understand the full effect. High injection pressure at low speed and low load caused an increase in the peak cylinder pressure and rate of heat release. This influence diminished as engine speed and load increased. The authors attributed this to the increased air mass flowing into the cylinder at higher speeds. The higher rate of air movement increased mixing and air density. In general, higher fuel pressures were shown to reduce BSFC. This was performed over a range of engine loads. BSFC with EGR was a little higher than without EGR. This is to be expected due to reduced oxygen concentration. CO and HCs were reduced with increased fuel pressure due to better atomization, leading to a shorter ignition delay and more complete combustion.

Ohishi et al. [26] reported the benefits of a Bosch HPCR system on the Duramax 6600 light truck engine. High injection pressures of 1600 bar were needed to keep injection duration short at high engine speeds, but still provide adequate amount of fueling. High injection pressure also helped keep particulate levels down by allowing injection timing to remain the same as the light load region. High injection pressure did increase combustion noise. However, this was mitigated by the use of pilot injection. Although specific to the Duramax 6600, the authors supplied an engine map with suggested injection pressures. *Figure 2.9* serves as an example for other modern diesel engines.

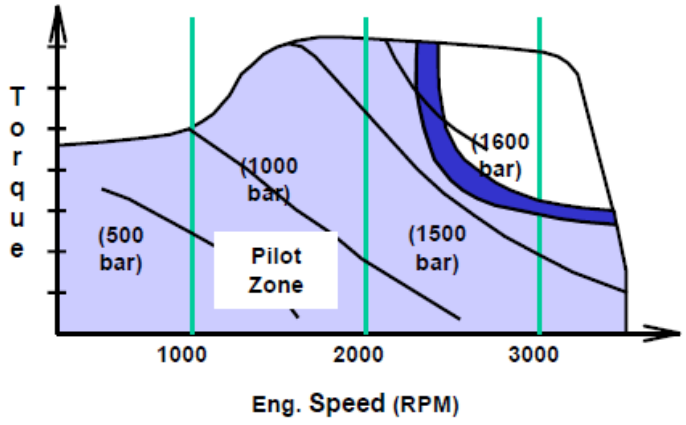

Figure 2.9: *Preferred injection pressures based on engine speed and load [10]*

Thirouard et al. [27] conducted an experiment to see high injection pressure or larger injector nozzle holes was a more effective method of increasing fuel flow rate. In both situations, increasing the fuel flow rate increased the speed of combustion. This allowed more time during the expansion process for soot post oxidation which reduced the overall soot levels. The added time in the expansion process also lowered the final exhaust temperature. High injection pressure was found to be preferred over larger injection nozzle holes especially at part load. At part load, larger nozzle holes increased the fuel-to-air ratio in the jet which increased soot emissions. The improved mixing of high injection pressure combined with higher fuel flow rate resulted in faster combustion. This allowed timing to be delayed closer to TDC which improved cycle efficiency.

2.3.2 Injection Rate Shaping

Injection rate shaping refers to the ability to define the profile of the quantity of fuel injected during the injection period. Typically, three major rate shapes are discussed which are square, ramp, and boot. *Figure 2.10, (a)* illustrates a boot, ramp, and square rate shape.

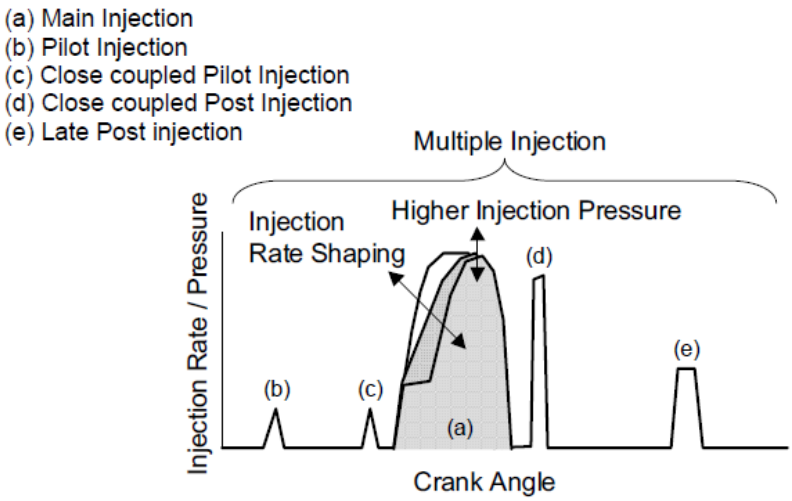

Figure 2.10: Rate Shape Examples [29]

By using different rate shapes throughout the engine operating map, many benefits are realized. Such benefits include reduction in noise levels [28], fuel consumption [29, 30], and exhaust emissions [29, 30, 34].

Carlucci et al. [28] studied changes in the fuel injection system as means of combustion noise control. This was done by comparing two HPCR injectors, a standard injector and one with a modified control valve to produce a ramp rate instead of square profile. Although changing parameters such as injection pressure and timing of the pilot had larger effects on the combustion noise, using a ramp rate shape had a measureable impact too. This reduced the amount of fuel injected during the ignition delay period which in turn lowered the peak cylinder pressures due to pre-mixed burn.

Tanabe et al. [29] used a HPCR system with two fuel rails to examine the effects of rate shaping in a multi-cylinder engine. The two fuel rails were plumbed together with one supplying high pressure fuel and the other low pressure fuel. By switching rapidly between the two rails, ramp, boot, and square rate shapes were produced without having to throttle at the injector nozzle. The authors found at high load and low or medium engine speed, the boot shape is favored while the square shape is preferred at high load and high speed. The ramp shape was preferred in the BSFC-Nox trade off at light load and low speed. Ramp and boot shapes were able to decrease Nox emissions because the amount of fuel injected into the cylinder during the ignition delay period was less than that of the square rate shape. This reduces the pre-mixed combustion and heat release rate which is responsible for lower Nox. The authors presented *Figure 2.11* as a summary of the optimal rate shapes throughout the engine operating map.

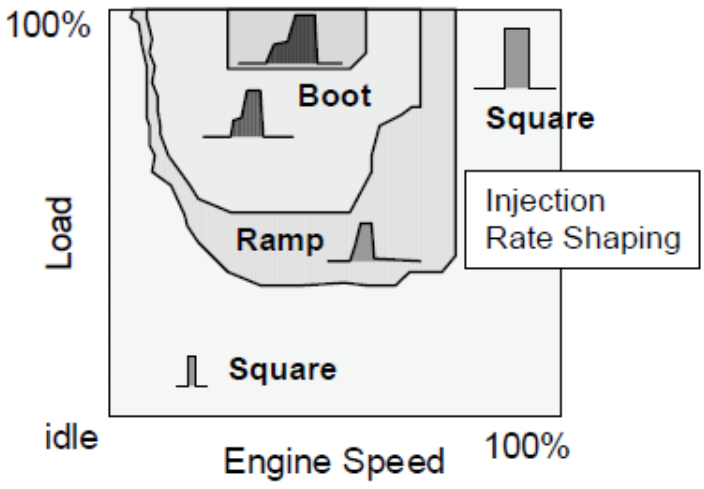

Figure 2.11: *Optimal Rate Shape Engine Map [29]*

Fischer et al. [30] compared a HEUI and HPCR system to see if rate shaping affected liquid length penetration. Liquid length is important to prevent wall-wetting which adversely affects emissions and fuel economy. It was found that rate shape had a negligible effect on liquid length. In addition, both injection systems were tested at two different injection pressures, 75 and 142 Mpa, but still no appreciable difference was found in liquid length.

2.3.3 Multiple Injections

In the past, diesel injection systems only offered a single main injection. However, modern injection systems can inject several times before and after the main injection. Some of the primary reasons for doing this are reduction of noise [31, 32], BSFC [32, 33, 34] and exhaust emissions [31, 32, 33, 34].

Zhang [31] showed pilot injection had the strongest affect at light load in reducing smoke and combustion noise level. According to Zhang, the benefit of pilot injection is due to shortening the ignition delay. The longer fuel is able to collect and mix, the stronger the premixed combustion. This results in a sharp rapid start of combustion as seen in *Figure 2.12*. At full load, boost pressure and fuel injection pressure are higher than light load. This shortens the ignition delay. Therefore, it was difficult for pilot to reduce the ignition delay further since it was already short at full load.

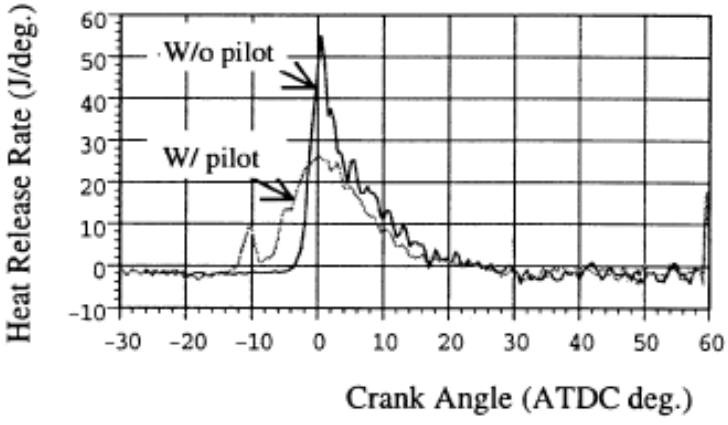

Figure 2.12: *Rate of Heat Release at 2200 RPM with 2 Nm Torque [31]*

Badami et al. [32] attempted several different injection strategies. Strategies included two pre-injections and a post-injection. Timings for the split injections were adjusted relative to main injection to find optimal injection timing. The post-injection was shown to reduce soot emissions, but did raise NOx slightly. The pre-injections were shown to reduce engine noise and BSFC.

Osada et al. [33] made comparisons with a single injection versus a main injection with a pre-injection and post-injection. The multiple injection strategy was shown to reduce BSFC by lowering heat losses to the wall with improved distribution of in-cylinder temperature. Also, a reduction in smoke was possible allowing for higher EGR rate. In turn, this produced lower Nox emissions as displayed in *Figure 2.13*.

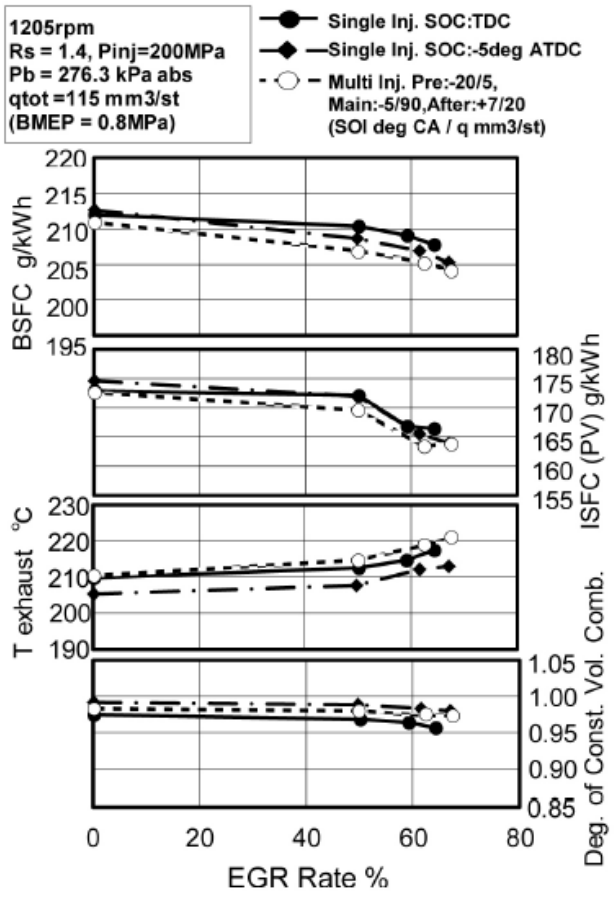

Figure 2.13: *BSFC reduction with pre-injection and post-injection [33]*

Aztler et al. [34] presented two different studies in one paper. First, multiple injections were used to reduce emissions and improve BSFC. Injection strategies investigated included single main, pilot and

main, main and post, and two pilots main and post. Pilot injection increased PM, but was able to reduce HC and CO. Pilot also gave a reduction in engine noise. A post injection was used to mitigate PM caused by the pilot. The second study focused on the effect of different ramp rates. It was found that the faster rate was always preferable. This is because the premixed combustion was reduced. Experiments were carried out with EGR. Results are summarized in *Figure 2.14* below.

Injection pattern	M (Main)	Pi+M	M+Po	Pi+Pi+ M+Po
PM g/h	0.6 1.2	4 5	1.1 1.6	2.7 3.4
ISFC g/kWh	219	217	215 217	209
CO g/h	60 72	40	65 70	24
HC g/h	5.2 5.0	4.0 3.5	6 5	2.5 3.1
dp/dα bar/°crk	5.0 5.5	5.3	5	3.1

Figure 2.14: Result using two different ramp rates combined with multiple injections [34]

2.4 CONCLUSION

In this paper, the benefits of the modern fuel injection system have been identified and explained. HEUI and HPCR injection systems were compared and a detailed description of their functionality and components was given. Through the literature review, the importance of the fuel injection system to have high fuel pressure, rate shaping control, and multiple injections was emphasized. The performance of the fuel injection system was shown to define the future of the modern heavy-duty diesel engine.

CHAPTER 3.0 : EXPERIMENTAL SETUP

3.1 TEST BED

3.1.1 Engine

The engine used in this research was a Caterpillar ACERT (Advanced Combustion Emissions Reduction Technology) C7. This engine was chosen because it is widely used in military vehicles including Stryker and MRAP (Mine Resistant Ambush Protected) family of vehicles. This engine utilizes a HEUI injection system and is capable of a maximum injection pressure of 180 MPa. Intake air is compressed by a fixed-geometry turbocharger with waste gate control. Since the charge air cooler is vehicle mounted equipment, an air-to-water charge air cooler of appropriate size was used to cool the intake charge. Engine cooling was handled by a tube-in-shell heat exchanger. For the purpose of data analysis and simulation work, the valve timing was needed. Since this is not published values, the valve timing was measured using a dial indicator. The procedure and values are listed in *Appendix A. Table 3.1* lists other significant engine characteristics.

No. Cylinders	6
Horsepower (hp)	330
Torque (ft-lbs)	860
Displacement (Liter)	7.24
Bore and Stroke (mm)	110 x 127
Compression Ratio	16.5:1

Table 3-1: CAT C7 Engine Characteristics

3.1.2 Dynamometer

Engine loading was performed by a Froude-Hofmann 350 kW AC dynamometer. 480 V, 3-phase electricity powered a VACON drive which controlled the dynamometer through a TEXCEL V[12] interface. Torque measurements were taken with a HBM-T40B inline torque meter. *Figure 3.1* shows the test bed setup.

Figure 3.1: Engine and Dynamometer Setup

3.2 DATA ACQUISITION SYSTEM

3.2.1 Overview

The data acquisition was composed of both a high-speed system and low-speed system. These two systems were synchronized by a common engine cycle number. *Figure 3.2* gives an overview of these systems. Their operation and equipment is described in detail in the following sections.

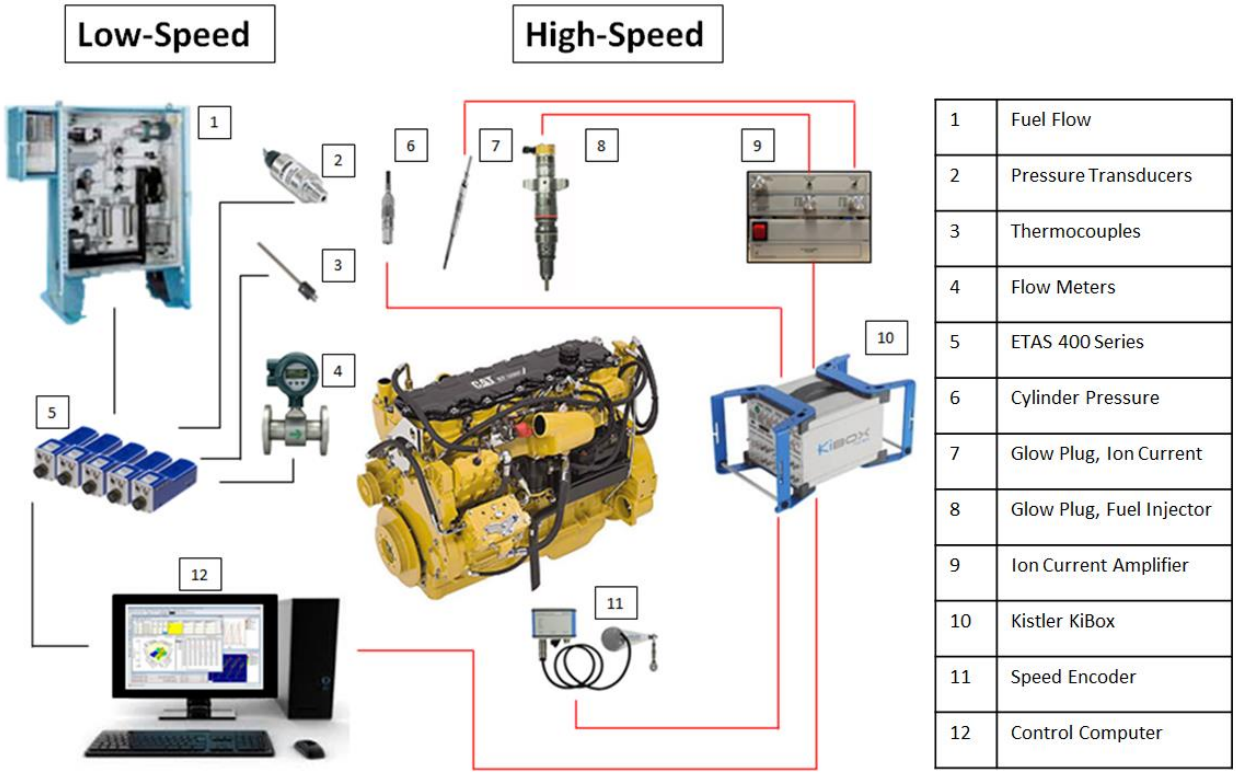

1	Fuel Flow
2	Pressure Transducers
3	Thermocouples
4	Flow Meters
5	ETAS 400 Series
6	Cylinder Pressure
7	Glow Plug, Ion Current
8	Glow Plug, Fuel Injector
9	Ion Current Amplifier
10	Kistler KiBox
11	Speed Encoder
12	Control Computer

Figure 3.2: Overview of Data Acquisition System

3.2.2 Low-Speed

ETAS hardware and software were used for the low-speed data acquisition. This system was chosen because of its seamless interface between the high-speed data acquisition and Bosch FlexECU. The low-speed system was synced to the high-speed system by sharing a common engine cycle number. INCA (version 7.1) was the software interface for the low-speed system. As well as handling data acquisition tasks, INCA communicated directly with a Bosch FlexECU. Plans to use this engine controller in future work would allow changing engine operating parameters and strategy.

Engine temperatures were measured with J-type thermocouples. Because of their temperature range, K-type thermocouples were used on the exhaust. Kulite pressure transducers were used to measure engine pressures. Yokogawa flow meters measured the water flow rate to the charge air cooler and engine coolant. A Pierburg PII 404 fuel flow meter measured engine fuel consumption. ETAS 400 series A/D converters connected these instruments to the control computer.

3.2.3 High-Speed

High-speed data acquisition was performed by a Kistler KiBox system. This device served as the charge amplifier for the piezoelectric cylinder pressure transducer as well as the signal processor for the crank angle encoder. The cylinder pressure transducer was a Kistler 6125C with a maximum pressure of 300 bar. Kistler also manufactured the 360 pulse-per-revolution (1 CAD) crank angle encoder (PN 2619A11). Through the KiBox, resolution of 0.1 CAD was possible through software interpolation. Data was recorded 100 engine cycles at a time.

Both the ion current sensing glow plug and fuel injector signals were recorded by the KiBox after being passed through a signal amplifier. This signal amplifier was built by Electro-Mechanical Associates. It offered a signal gain 50 for up to two channels with a response frequency of 10 kHz. In addition, ion current potential voltage could be set from 0-100 VDC and polarity reversed. In this work, all experiments were conducted with +100 VDC connected to the ion current sensor.

3.3 HARDWARE MODIFICATIONS

In order to take in-cylinder measurements, instrumentation bores were necessary to accommodate the cylinder pressure transducer and ion glow plug sensor. Since the CAT C7 uses an intake heater for cold starting rather than a glow plug, there was no previous bore to modify for the ion glow plug sensor. Caterpillar graciously assisted in providing the location they use for installing cylinder pressure transducers for research purposes. Typically, they install cylinder pressure transducers behind the fuel injector. In addition to this bore, another site was still needed for the location of the ion glow plug sensor. Finding a safe location was a challenging task for many reasons. First, the HEUI injector is very large in diameter. Second, the injector is installed in the cylinder on a compound angle. This eliminated options of making a simple straight bore because of the area affected by the injector's path. Third, the location for the instrumentation bore had to avoid the direct spray of the fuel injector. Not only would disrupting the spray affect engine performance, but ion current measurements would be negatively impacted if the sensing tip was wetted by liquid fuel. Lastly, the cylinder head is very complicated due to the many

regions that must be avoided. Because of the HEUI system, there is a fuel rail and oil rail that run through the center of the cylinder head. In addition, the two intake runners and single exhaust runner must also not be penetrated by the instrumentation bore.

To find a second location for an instrumentation bore, a damaged cylinder head was cut into several sections. Cylinder six was removed from the head and cut again down the centerline of the injector bore. This revealed the locations of the intake runners, exhaust runner, fuel rail, oil rail, and cooling passages. After the locations of these elements were identified, the spray pattern of the injector had to also be taken into account. An injector was installed in the head with the nozzle holes marked. Six lines were drawn 60 degrees apart from each to represent the injector spray pattern as can be seen in *Figure 3.3*. After extensive measurements, a second site for an instrumentation bore was located. A straight bore through a cylinder head casting plug led directly to the outer edge of the combustion chamber. From the bottom side of the cylinder head, *Figure 3.3* displays the location for the instrumentation bore behind the injector and the second instrumentation bore through the casting plug. This picture was taken before the bores were actually machined. *Figure 3.4* shows the two machined bores from the top side of the cylinder head.

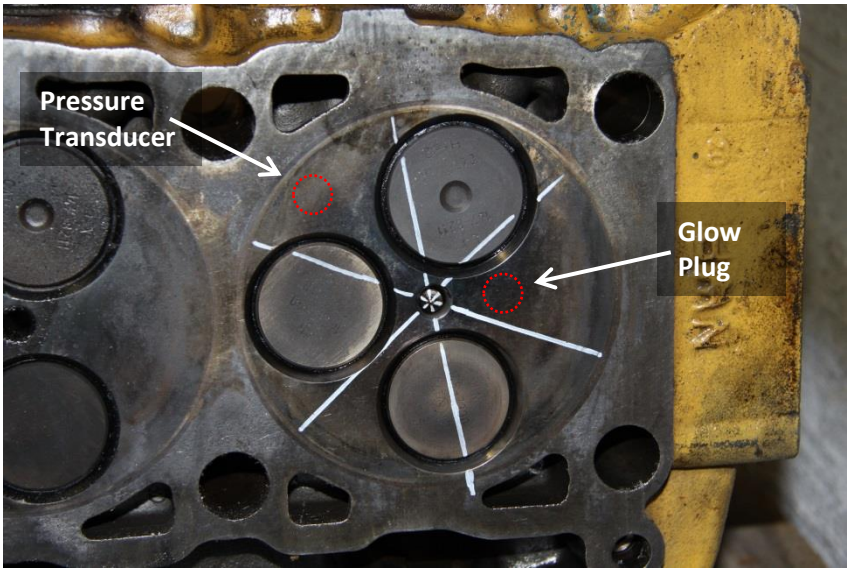

Figure 3.3: Bottom Side of Cylinder Head

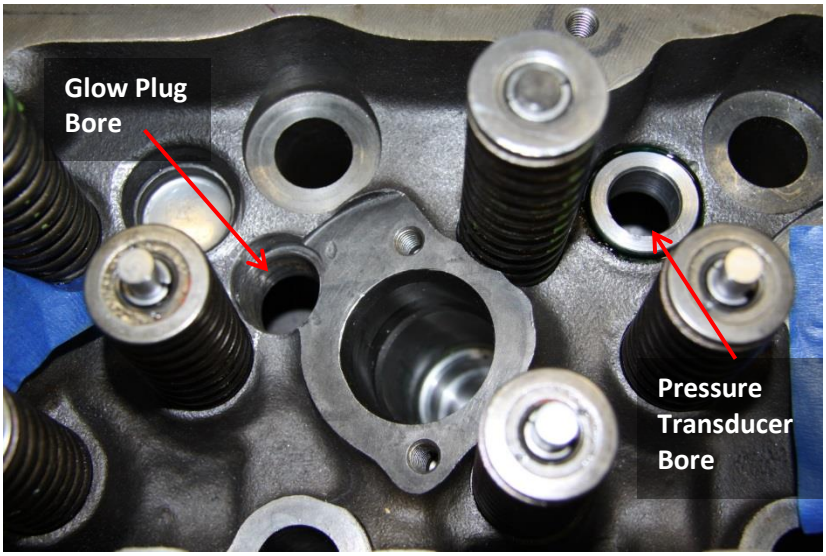

Figure 3.4: Top Side of Cylinder Head

Although Caterpillar originally provided details for placing a pressure transducer in the cylinder head behind the injector, it was decided to exchange this position for the glow plug ion sensor. This decision was made for two reasons. First, the glow plug ion sensor penetrated into the combustion chamber approximately 3-5 millimeters. Having the glow plug ion sensor near the injector insured the sensor was in the combustion bowl. With the tip of the sensor in the combustion bowl, the possibility of contact between the piston and sensor at TDC was minimized. Another reason for moving the glow plug sensor closer to the injector was the strength of ion current would be strongest in the combustion bowl. Unlike cylinder pressure, ionization is a local measurement. While moving the pressure transducer near the cylinder wall did not affect the cylinder pressure measurement, the amplitude of the ion current signal would have been negatively impacted.

Since both the instrumentation bores penetrated cooling passages inside the cylinder head, sleeves were used to seal the coolant from the combustion chamber and from mixing with engine oil. These sleeves were threaded into the firing deck of the cylinder head. A copper crush washer prevented combustion gases from leaking past the threaded sleeve. At the top end, an O-ring acted as a barrier keeping coolant from entering the valve train and mixing with engine oil. Both the threaded portion and

O-ring were coated with an anaerobic sealant (Loctite 680) as an additional measure of protection. *Figure 3.5* shows both the pressure transducer and glow plug ion sensor sleeves.

Figure 3.5: Pressure Transducer Sleeve (Left) and Glow Plug Sleeve (Right)

3.4 ION SENSOR DESIGN

3.4.1 Glow Plug Ion Sensor

Since the CAT C7 does not use glow plugs for cold-starting, a market search was conducted for the thinnest metal-tipped glow plugs available. Thin glow plugs were desirable because this increased the space available between the glow plug and instrumentation sleeve for insulation. Metal-tipped glow plugs were necessary, as opposed to ceramic, because a good electrical conductor was needed to carry the ion current signal. Bosch glow plugs (PN 0250403008-4N3) were selected to be modified for ion current sensing.

In order for the glow plug to retain its heating function while also being an ion current sensor, an additional wire needed to be attached to the glow plug. Normally, the glow plug harness is a single wire harness carrying a positive voltage. The circuit is completed through the glow plug body through the cylinder head and then back to battery ground. However, since the glow plug was insulated from the cylinder head for the purposes of detecting ion current, a second wire was attached to act as the ground. This was accomplished by press fitting a copper sleeve onto the threaded portion of the glow plug. The copper sleeve served as a base to which the ground wire was soldered. This was then covered with heat shrink for protection. Since the instrumentation sleeve was longer than the glow plug, the positive terminal was extended. Two methods were tested for extending the positive terminal. First, a small hole

was drilled in the terminal. The wire was inserted into the hole and they filled with solder. Another method involved brazing a steel rod onto the terminal. An example of the wire/copper sleeve method is displayed in *Figure 3.6* while *Figure 3.7* shows the brazed rod method.

The ion current glow plug was retained in the instrumentation sleeve using a threaded plug with a locking nut. The threaded plug had a bore through the center which allowed the leads to pass out. An insulated lower and upper bushing kept the ion current glow plug from touching the instrumentation sleeve walls. The upper bushing also provided a surface for the threaded plug to tighten against. *Figure 3.7* shows the components used to retain the glow plug.

Figure 3.6: Ion Current Glow Plug with Attached Wires

Figure 3.7:Ion Current Glow Plug with Brazed Rod

CHAPTER 4.0 : EXPERIMENTAL DATA AND ANALYSIS

4.1 DESCRIPTION OF MEASUREMENT CONDITIONS

4.1.1 Data Sampling and Presentation

The experimental data presented in this thesis were acquired at 3600 pulses per revolution (0.1 CAD). The cylinder pressure traces and ion current signals presented in this paper are the raw signals. However, these signals have been averaged over 100 engine cycles. This was done to remove noise and the effect of cycle-to-cycle variability. In calculating the RHR (Rate of Heat-Release), a low-pass Fourier filter (roll-off start = 2000 Hz, end = 3360 Hz) was used to remove signal noise from the cylinder pressure transducer.

4.1.2 Engine Operating Mode

As described in Chapter 2, the HEUI system is capable of multiple injections and rate shaping. The HEUI system employed on the research engine in this study was also capable of multiple injections and rate shaping. However, in order to simplify the analysis of the experimental results, the engine was operated under a single injection event. The engine was set in this mode by replacing the coolant temperature sensor with a resistor. Since the resistor held a constant value regardless of actual engine temperature, the Caterpillar ECU operated the injection system in the "cold mode" parameters. This mode affected both the injection timing and also the number of injections. In this way, the production ECU allowed for a comparison of different engine loads while still using a single injection event. Otherwise, the number of injection events would have changed from light loads to high loads.

As the experimental data is reviewed, it is important to keep in consideration the engine was in "cold mode", not the Caterpillar production injection strategy. At medium and high loads, the duration of the single injection continues into the diffusion burn portion of combustion. Traditionally, this is very undesirable for the sake of emissions, specifically for soot production. The benefit of multiple injections and rate shaping over a single injection event in a HEUI system has been described in detail by Caterpillar [19]. *Figure 4.1* gives an overview of the advantage of multiple injections and rate shaping. Since the

focus of this work was not a study of the emissions of this engine, the simplicity of a single injection for data analysis was preferred over the higher soot output.

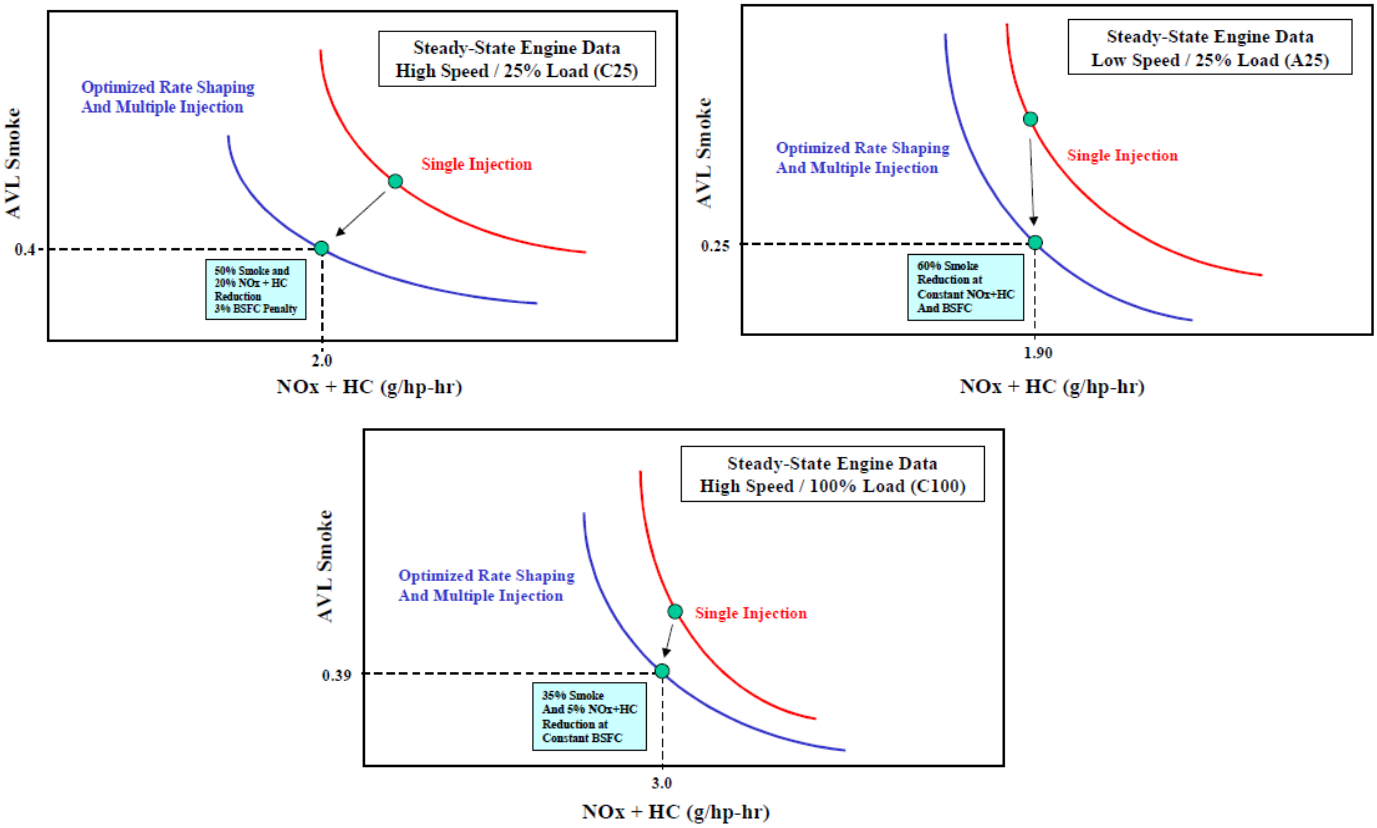

Figure 4.1: Soot Comparison for Optimized Injection Strategy [19]

4.1.3 Description of Example Data

In the same engine cylinder, simultaneous recording of cylinder pressure, ion current from the glow plug, ion current from the fuel injector, and injection command was possible. Although this capability was resident in the engine, often issues with the one of ion current probes prevented simultaneous recording. However, in all figures in this work where ion current from the glow plug and ion current from the injector are presented together, the data was recorded simultaneously. *Figure 4.2* demonstrates a recording session of the full set of in-cylinder instrumentation over a complete engine cycle. This data was recorded at an engine load of 85 ft-lbs at 1000 RPM.

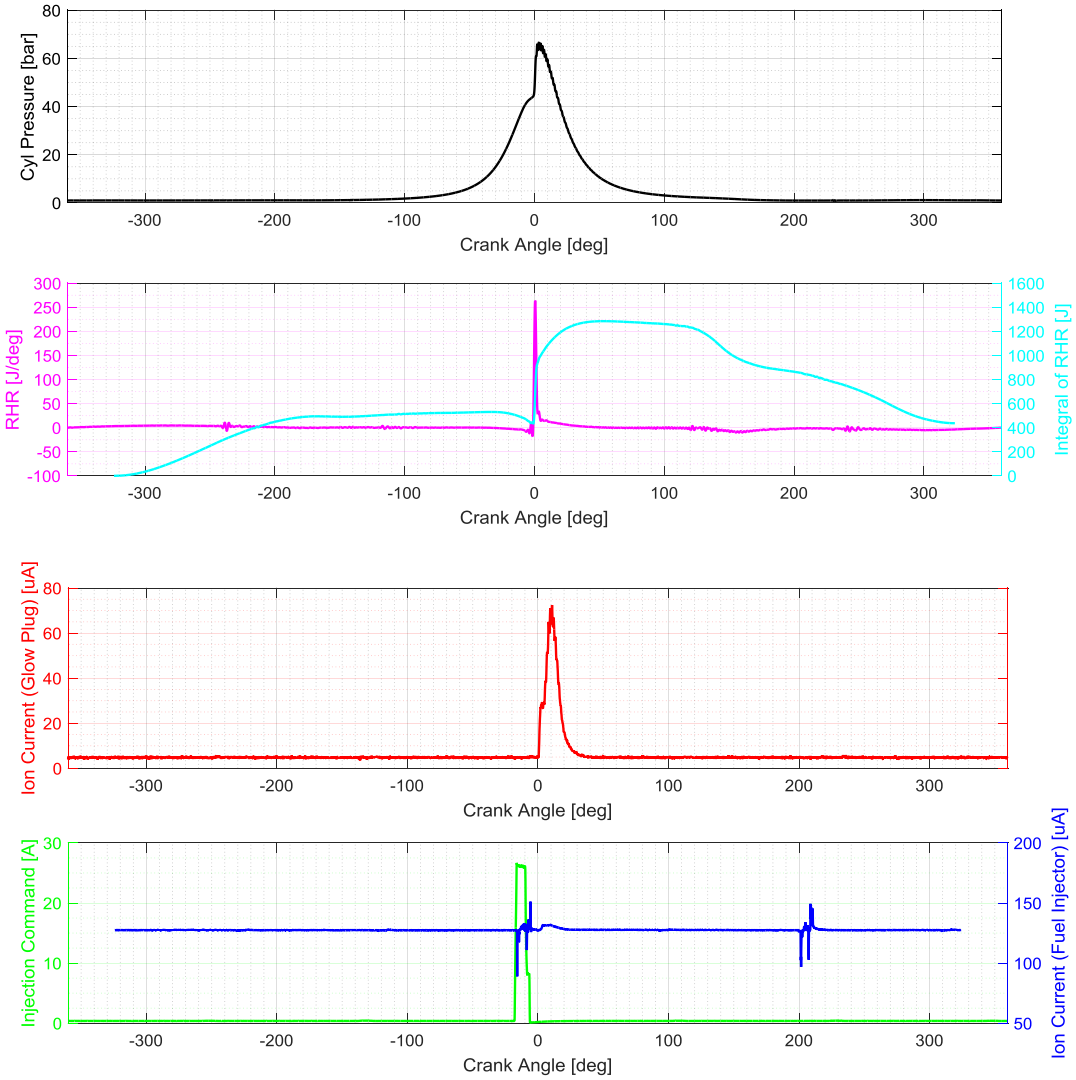

Figure 4.2: 85 ft-lbs at 1000 RPM, Full Cycle

The data represented in *Figure 4.2* is displayed again in an expanded view in *Figure 4.3*. From this perspective, the details of the combustion process can be described in detail.

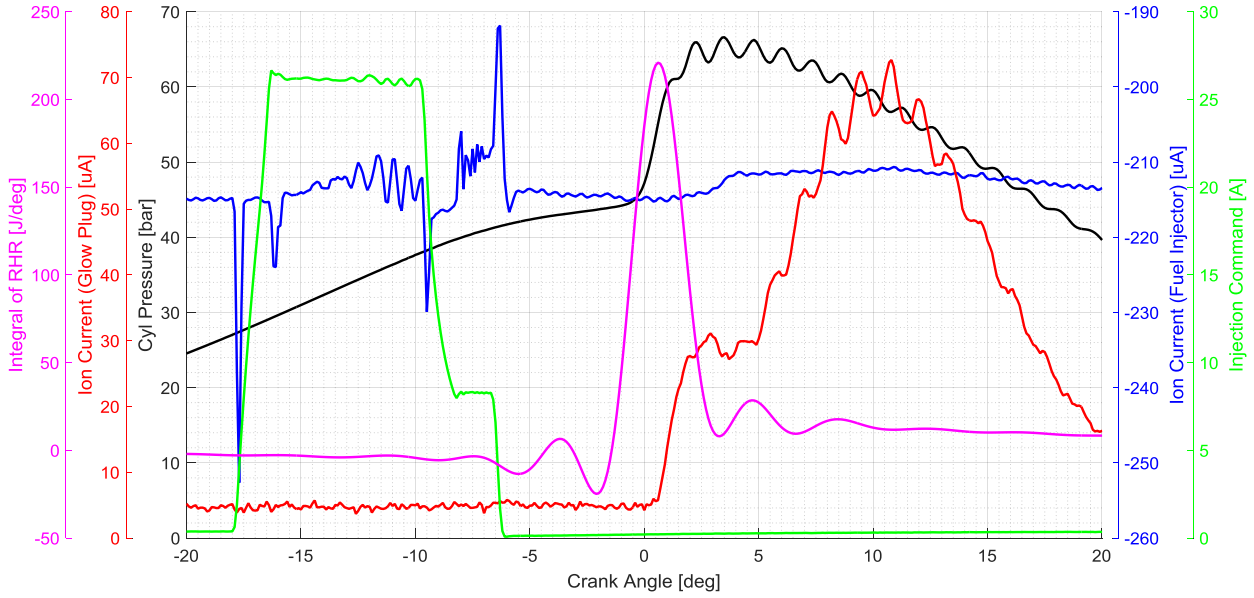

Figure 4.3: 85 ft-lbs at 1000 RPM, Expanded View

For this engine speed and load, the location of peak cylinder pressure occurred at 3.5 CAD ATDC. The command for fuel injection began at -17.9 CAD BTDC and ended at -6.2 CAD BTDC. Since the injection command was early and short in duration, lasting only 11.7 CAD, the resulting combustion was mostly premixed combustion. This is evidenced by the large peak located in the RHR curve occurring at 0.5 CAD ATDC. A predominantly premixed combustion is expected since the engine load was light and fuel finished delivery before TDC. A small peak in the RHR at 3.3 CAD ATDC represents the diffusion burn portion of combustion. This peak becomes predominant as engine load increases. The ion current measured by the fuel injector detects the actuation of the solenoid in the fuel injector. Peaks in this signal occur at the same timings as the fuel injection command. This behavior is described with greater detail in the following section devoted to the fuel injector ion current. Combustion is detected by the fuel injector ion current beginning 2.4 CAD ATDC. This is later than the glow plug ion current signal which detected combustion at 0.6 CAD ATDC. This time shift can be explained by the position of the glow plug ion current sensor. Since this sensor was deeper in the combustion bowl and closer to the wall, it is likely combustion began there first. At the perimeter of the combustion bowl, the liquid fuel jet has begun to evaporate and is the first to ignite. The glow plug ion current signal also had a higher rise in its peak. This can be attributed to the glow plug's larger surface area than the fuel injector.

4.2 EFFECT OF ZERO-SHIFT

In both the fuel injector and glow plug ion current signals, the effect of zero-shift was present. Zero-shift is defined as the increase in the baseline of ion current over time. The ideal ion current signal would return to the zero crossing when combustion has completed. However, over time a shift is witnessed which causes the ion current signal to increase even though combustion is not taking place. Zero-shift occurs for two main reasons. First, the ion current probe can be covered with soot which can cause a short to ground. As discussed in the "Engine Operating Mode", the experiments were conducted using a single main injection. This causes a high amount of soot production. As the buildup of soot increases, so does the effect of zero-shift on the ion current signal.

The second reason zero-shift occurs is due to a breakdown in ion current sensor insulation. As the insulation breaks down, a high resistance path to ground is created. Over time, the resistance decreases and the flow of the ion current increases. Engine load proved to have a great effect on the breakdown of ion current sensor insulation. The increased cylinder pressure at medium and high loads caused the insulation to fail rapidly. In addition, the medium and high loads also caused increased temperature in the cylinder head. High temperatures caused the dielectrics in the ion current sensor to lose their insulating properties.

The occurrence of zero-shift can be categorized two different ways: within the same test point or between test points. If zero-shift develops within the same test point, this usually is a sign that the ion current sensor's insulation is deteriorating rapidly. Often, a complete electrical short follows quickly. *Figure 4.4* is an example of this. In this figure, 100 engine cycles of the same test point are displayed. In the last 30 engine cycles, the ion current baseline diverges from the other engine cycles for this test point. When zero-shift happens within a cycle, it must be identified to be properly accounted for during data processing. In this study, when zero-shift occurred near the end of data collection at a given test point, engine cycles which diverged from the majority were disregarded.

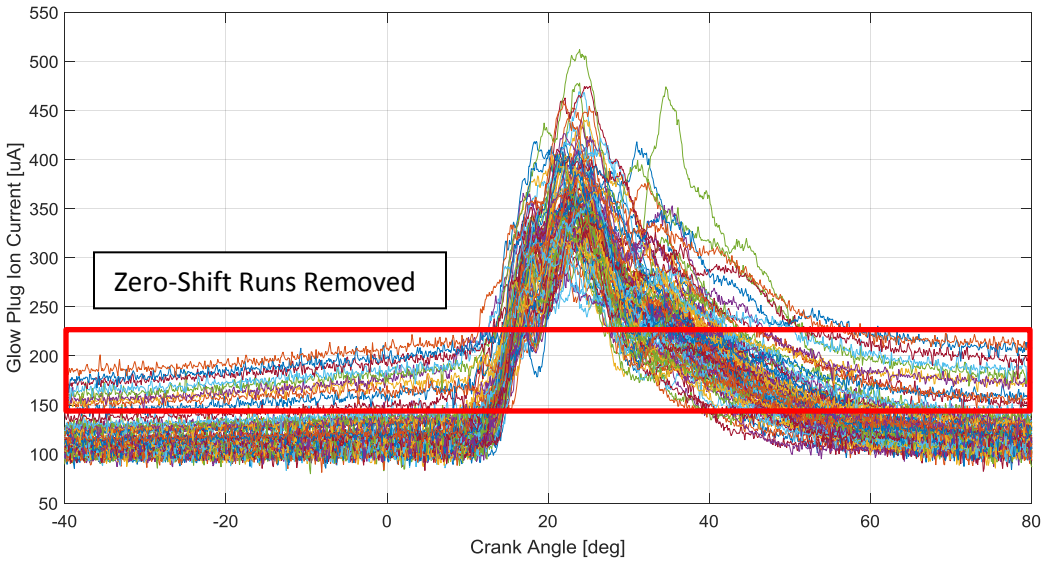

Figure 4.4: Example of Zero-Shift within a Test Point

The second category of zero-shift takes place at the transition to a new test point. The increase of cylinder pressure due to increased load often causes additional stress on the ion current sensor's insulation. *Figure 4.5* illustrates zero-shift for fuel injector ion current while *Figure 4.6* glow plug ion current zero-shift. Correcting zero-shift between test points can easily be handled in data processing. An offset can be applied to bring the signals to a common base. In the following sections describing ion current characteristics, offsets were applied to better visualize the effect of changing engine load has on amplitude and other features.

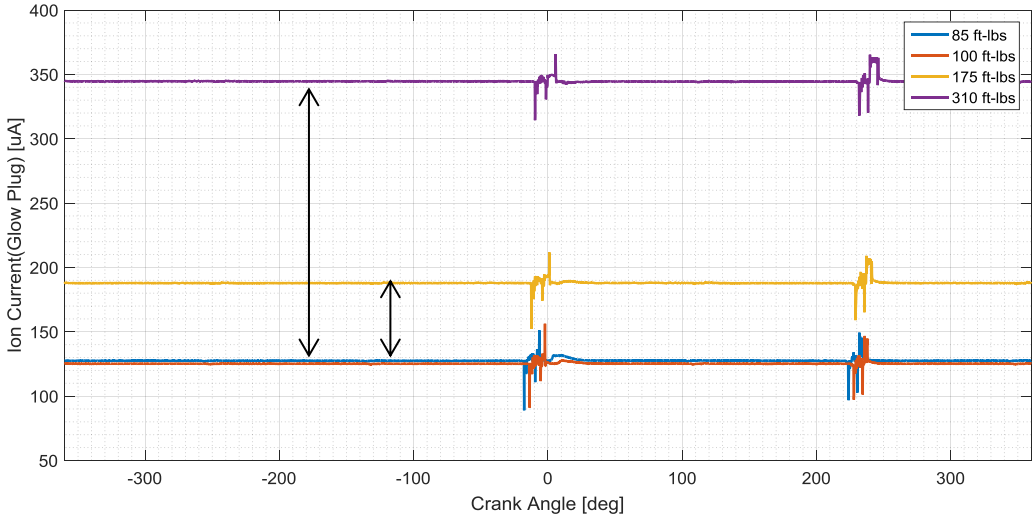

Figure 4.5: Zero-Shift in Fuel Injector between Test Points

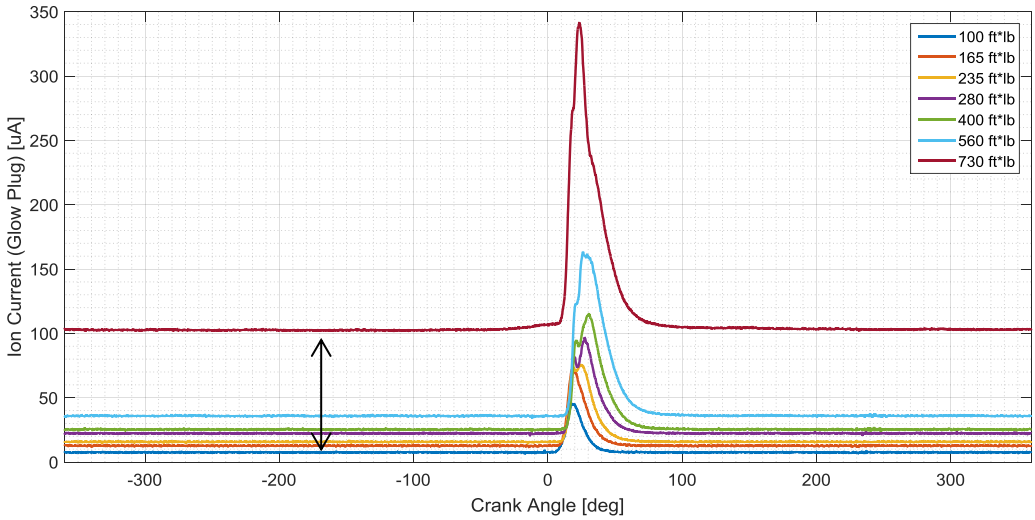

Figure 4.6: Zero-Shift in Glow Plug between Test Points

4.3 FUEL INJECTOR ION CURRENT CHARACTERISTICS

Although fuel injectors previously have been converted into ion current sensors, these have been of the HPCR type. The HEUI fuel injector proved to be especially challenging to modify for this purpose. Since HEUI fuel injector has separate regions that need to seal against oil and fuel, the number of surfaces to insulate increase. In addition, the tight tolerances cause several different types of insulating coatings to scratch, tear, or crack during the fuel injector installation. Due to these issues, only a limited set of data from the fuel injector was collected.

4.3.1 Ion Current as a Fuel Injection System Diagnostic

During the process of recording ion current measurements with the fuel injector, an unexpected discovery was made. Throughout the time period of the injection command from the ECU, there was a disturbance in the ion current signal measurement. Initially, this was attributed to signal noise distorting the measurement. However, under closer examination, it turned out to be useful information. By energizing the fuel injector with a voltage potential, not only the ion current was detected, but also the electrical signature of the injector solenoid and injector driver. This signature was very repeatable and reliable with features in the ion current signal. In fact, all major events in the injection command relates to either a rising or falling peak in the ion current signal. *Figure 4.7* displays the influence of the injection command on the ion current signal.

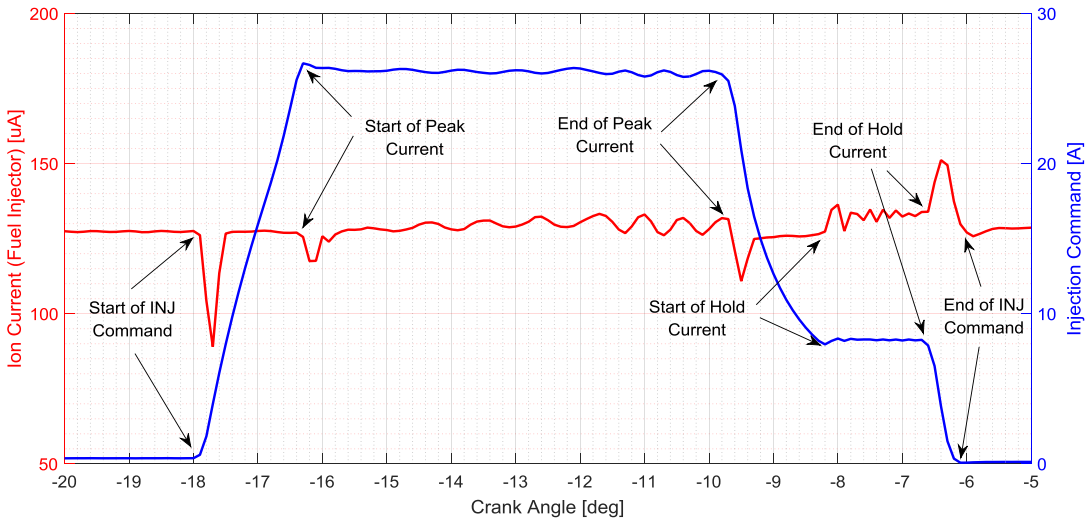

Figure 4.7: Comparison of Injection Command to Injector Ion Current Signal

From *Figure 4.7*, the start of injection command, start of peak current, end of peak current, start of hold current, end of hold current, and end of injection command can all be clearly discerned using the ion current signal. To further emphasize this point, *Table 4.1* gives the CAD degree for each of these events. By reviewing this table, the accuracy of the ion current signal to model the injection command is proven. In most cases, there exists only 0.1 CAD offset between the injection command and the ion current signal.

Injection System Event	Injection Command	Ion Current
Start of Injection Command	-18 CAD	-17.9 CAD
Start of Peak Current	-16.3 CAD	-16.4 CAD
End of Peak Current	-9.8 CAD	-9.7 CAD
Start of Hold Current	-8.2 CAD	-8.2 CAD
End of Hold Current	-6.7 CAD	-6.6 CAD
End of Injection Command	-6.1 CAD	-5.9 CAD

Table 4-1: Comparison of Injection Command to Fuel Injector Ion Current

In addition to being able to detect the signature of the injector solenoid and injector driver in cylinder 5, the instrumented cylinder, the signature was also detected for cylinder 6. This was discovered when viewing a full engine cycle, not just the region surrounding combustion. *Figure 4.8* shows two electrical signatures. The first one occurs in cylinder 5 and has the accompanying injection command as recorded by a current clamp. The second signature occurs at approximately 240 CAD. This was identified as cylinder 6 since the engine's firing order is 1-5-3-6-2-4. Due to the firing order, an offset of 240 CAD is expected.

From the literature review, Estefanous [36] attributes the detection of the electrical signature to the Hall Effect. Interestingly, cylinder 5 detected the electrical signature of cylinder 6, but not cylinder 4. Since cylinder 5 is equidistant from cylinder 4 and cylinder 6, it was clear that the electrical signature of cylinder 6 was not transmitted by the fuel injector solenoid through the air. After investigating the engine electrical harness, it was found that both cylinder 5 and 6 share a common ground. Therefore, a reflection of the energizing of the fuel injector solenoid by the ECU injector driver in cylinder 6 was transmitted through the common ground back to cylinder 5.

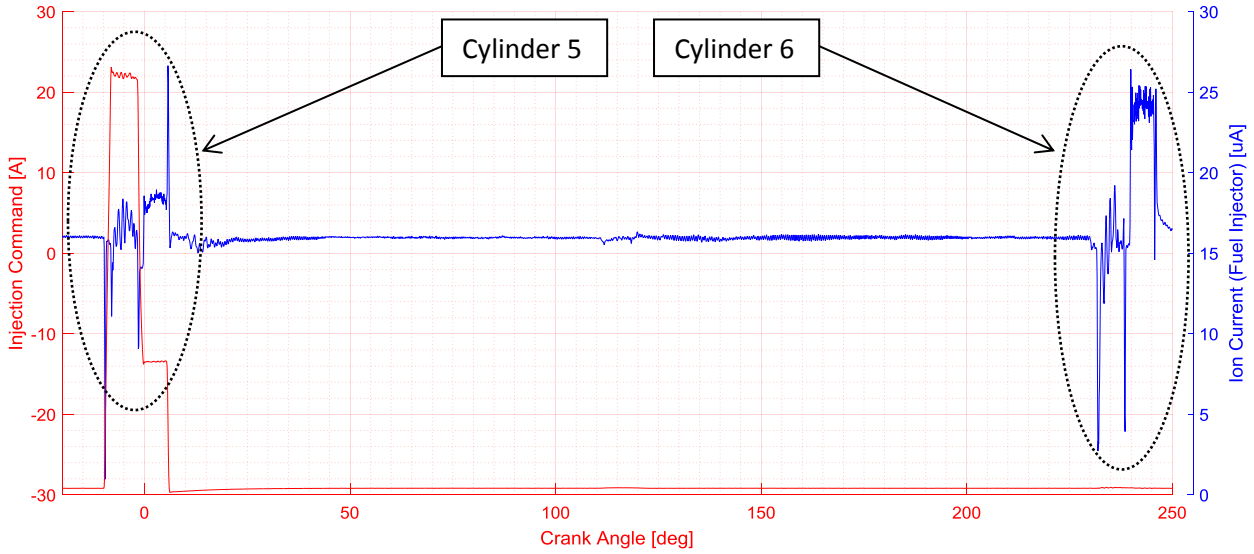

Figure 4.8: Electrical Signature of Cylinder 5 and 6

The application of this discovery could be leveraged as a diagnostic for the HEUI fuel injection system. Using an ion current sensing fuel injector, details about the injection system can be determined. Specifically, during an engine malfunction, the failure between a bad injector driver in the ECU or a bad fuel injector solenoid can be distinguished. Since the ion current fuel injector senses multiple cylinders, problems occurring in more than one cylinder can be attributed to the injector driver. Otherwise, the failure can be isolated to an individual cylinder and assumed to be an issue with the fuel injector solenoid. In addition, by examining the rise and fall of the ion current signal around the injection command, the health of the injector driver or solenoid can be evaluated.

4.3.2 Effect of Engine Load on Ion Current

Unfortunately, a limited amount of data was available from the fuel injector ion current sensor. Due to issues insulating the injector, the desired investigation to determine the effect of engine load on ion current was cut short. Only four engine loads (85, 100, 175, and 310 ft-lbs) at a 1000 RPM were recorded. The results are shown in *Figure 4.9* below.

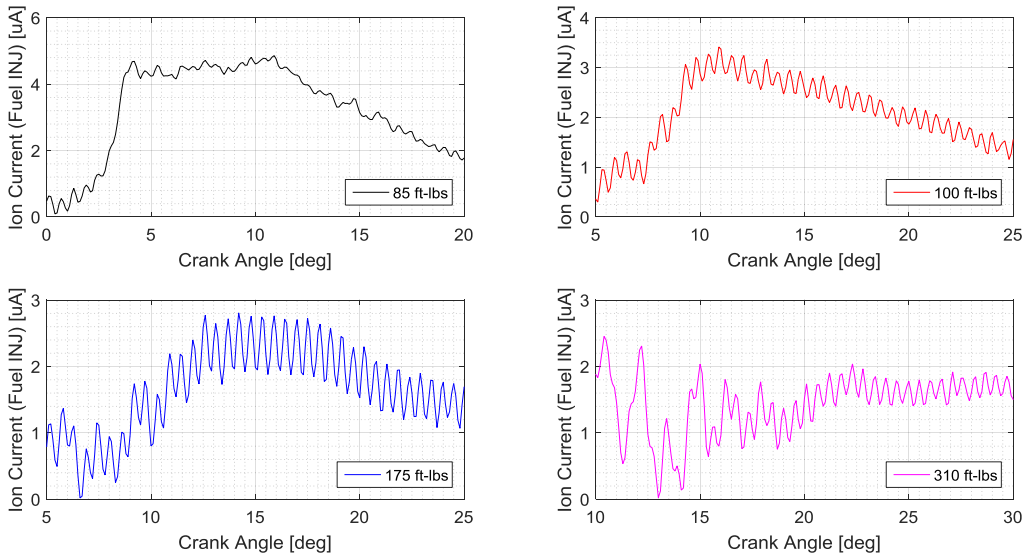

Figure 4.9: Injector Ion Current at 1000 RPM

In examining the above plots, there are several unusual observations. First, the amplitude of the ion current is supposed to increase with engine load. Although this relationship was followed by the glow plug ion current sensor, the inverse was true in the fuel injector ion current sensor. Second, the amplitudes of the ion current signals were much lower that the glow plug ion current sensor. While the fuel injector ion current signal ranged from 0 – 5 µA, the glow plug ion current signal ranged from 0 – 70 µA for similar engine loads. Third, the 310 ft-lbs test point did not detect an ion current signal. Lastly, except for the 85 ft-lbs test point, there was a high frequency oscillation on top of the ion current signal.

The lack of success in the fuel injector ion current signal is attributed to several reasons. First, the detection of the ion current signal from the fuel injector was intermittent. Although many insulation methods were attempted on the fuel injector, the search for a satisfactory solution is still ongoing. These methods include ceramic paint, dielectric coatings, and fiberglass tape. In *Appendix B*, a complete listing of coatings used for insulation for the fuel injector is provided for reference. Since the data presented here is the average of 100 engine cycles, engine cycles where no ion current is detected lowers the average amplitude.

Second, it is suspected there is an interaction between the glow plug and fuel injector ion current sensors. Although other researchers in the literature have used multiple ion sensors in the same cylinder,

typically the sensors have been of similar design. Since the surface area and penetration of the glow plug versus the fuel injector are very different, it is reasonable to believe that there was a greater attraction by the glow plug than the fuel injector. From the chemical and thermal processes which create ions, only a finite number are present in the combustion gas each engine cycle. If the attraction of the glow plug is higher than the fuel injector, the ions will flow through the path of least resistance. Therefore, the majority of the ions would be collected by the glow plug ion sensor which in turn decreases the available amount to be detected by the fuel injector ion sensor. Unfortunately, damage to the fuel injector insulation prevented running tests to validate this theory.

Lastly, the electrical signature produced by the fuel injector solenoid and injector driver over runs the ion current signal at medium and high loads. This can be easily seen from *Figure 4.10* which represents the 310 ft-lbs test point. From the RHR curve, the peak of premixed combustion occurred at 4 CAD which was within the period of time that the fuel injector was still injecting fuel. Attempting to measure ion current while the fuel injector solenoid is energized results in distortion of the ion current signal by the electrical signature of the solenoid and driver. Although the electrical signature from the fuel injector solenoid and driver can be used as a diagnostic, it presents a limitation when trying to measure ion current.

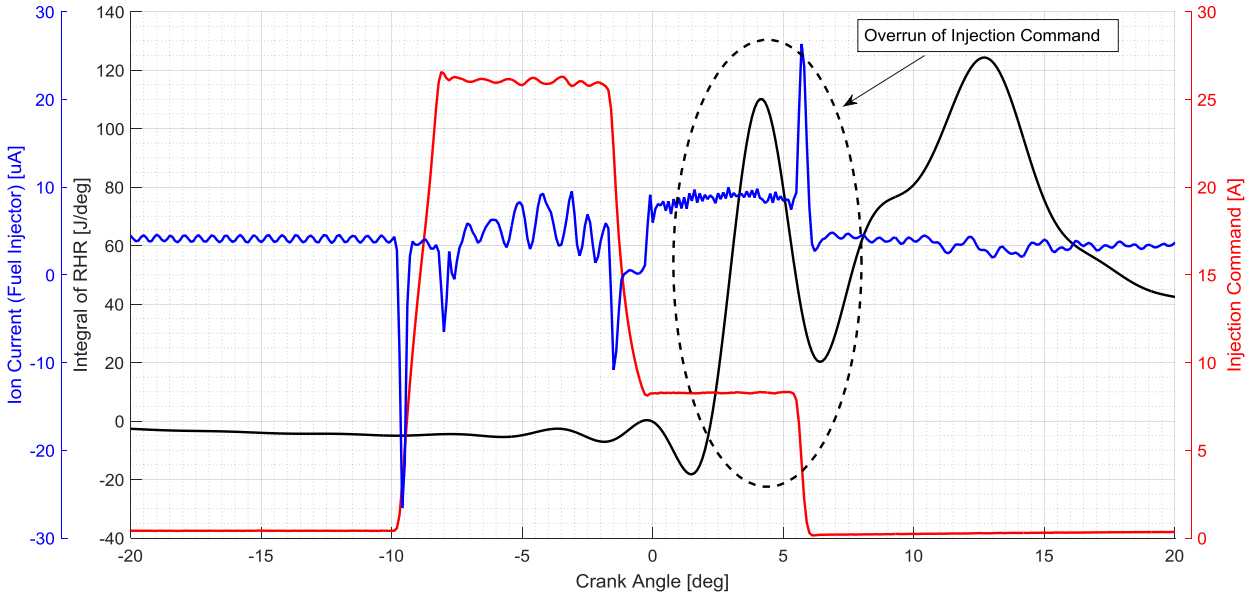

Figure 4.10: Overrun of Electrical Signature into Combustion

4.4 GLOW PLUG ION CURRENT CHARACTERISTICS

Ion current measurements obtained from the ion sensing glow plug provided a much more reliable signal than that of the fuel injector. This is primarily because the geometry of the body of the glow plug which made insulation much simpler than the complex shape of the fuel injector. If a more durable method for insulating the fuel injector been discovered, the results from both the glow plug and fuel injector should have been very similar.

4.4.1 Effect of Injection Timing on Ion Current

Since this study was performed on the production Caterpillar ECU, the start of injection was not able to be held at a fixed timing. Although the actual start of the fuel spray was not known due to the spool valve delay in the HEUI fuel injector, the start of the fuel injection command was recorded through a current clamp. *Figure 4.11* presents the fuel injection commands for the glow plug ion current test points. *Figure 4.12* shows the change of injection duration with engine load.

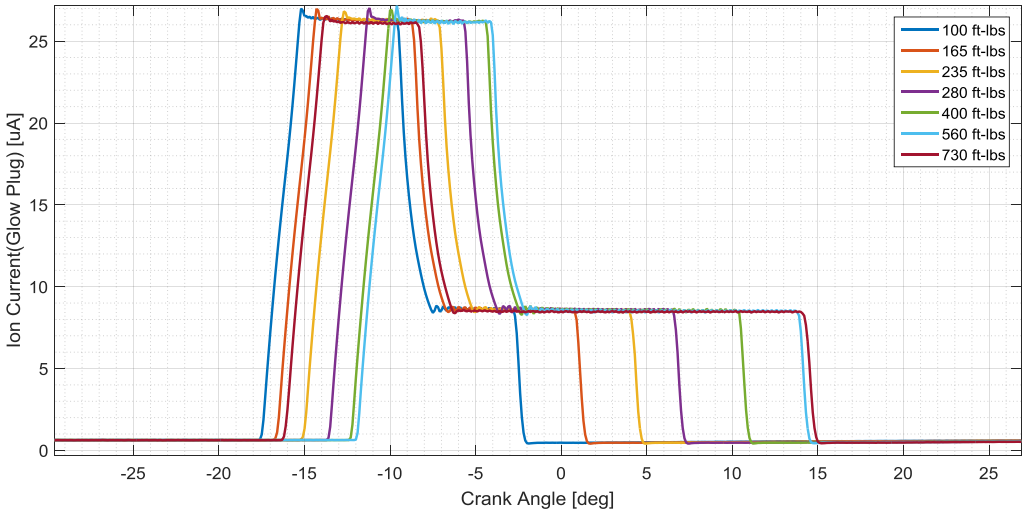

Figure 4.11: Change in Injection Timing with Engine Load

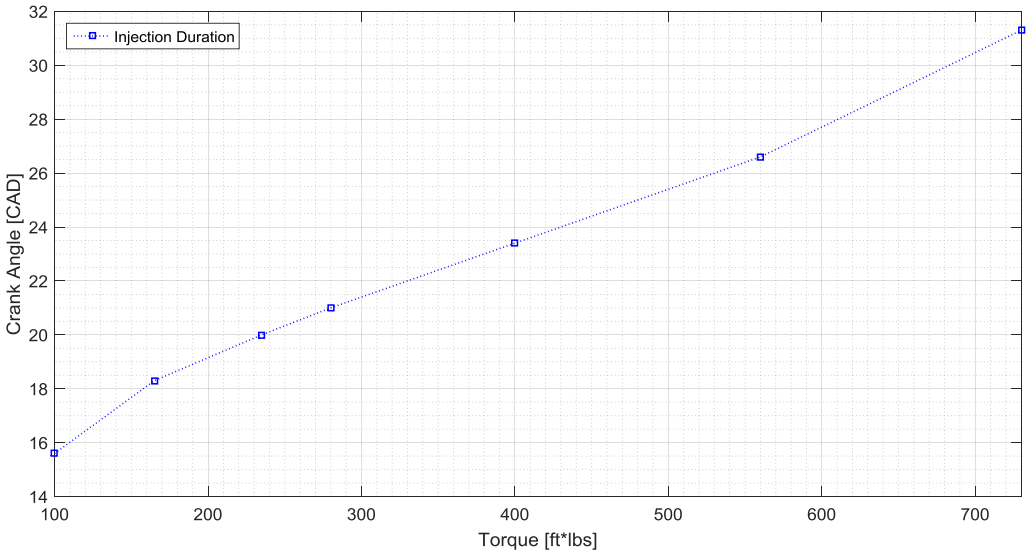

Figure 4.12 Change in Injection Duration with Engine Load

From *Figure 4.11*, SOI (Start of Injection) moved steadily closer to TDC with increasing engine load except for the highest load point, 730 ft-lbs. However, this point still had the latest EOI (End of Injection). The SOI for 730 ft-lbs broke the trend from the other load points because it was the only way to continue increasing injection duration without introducing fuel too late in the expansion stroke. As expected, *Figure 4.12* shows the injection command duration increasing with engine load. Longer

injection duration is required to place more fuel in the cylinder to perform at heavy loads. The end of injection steadily grew as the duration of injection increased.

In order to identify the influence of the start of injection command over ion current, a reference point in the ion current signal was needed. In the literature, Badawy [3] determined that the SOIC (start of ion current) was the most reliable parameter in the ion current signal. He defined the SOIC by first finding the value of the ion current signal at SOI. The value of the ion current at SOI set the threshold for deciding SOIC. The threshold was increased by 20% to separate the rise of ion current from other signal noise. In addition, a 0.2 μA offset prevented threshold from being a negative value if the signal noise was below the zero crossing at SOI. *Equation 4.1* is the described expression for determining SOIC.

$$SOIC = [Threshold(@SOI) + 0.2\mu A] * 120\% \qquad (4.1)$$

By using Badawy's expression, a consistent method for determining SOIC was provided. This offered a basis for making a correlation between SOIC and SOI. Since the Caterpillar production ECU was used in these experiments, SOI was not able to be held constant. This prevented a direct comparison of the SOI to SOIC. To resolve this, the delay between these two points was compared. The SOIC delay was calculated as the sum of the absolute values of SOI and SOIC. This parameter gives the number of CAD between SOI and SOIC. *Figure 4.12* summarizes the SOI, SOIC, and the delay in SOIC. A linear trend line was fitted to the delay in SOIC curve. This shows the consistency of the delay in SOIC with change of engine load. *Table 4.2* gives the actually CAD for these injection events.

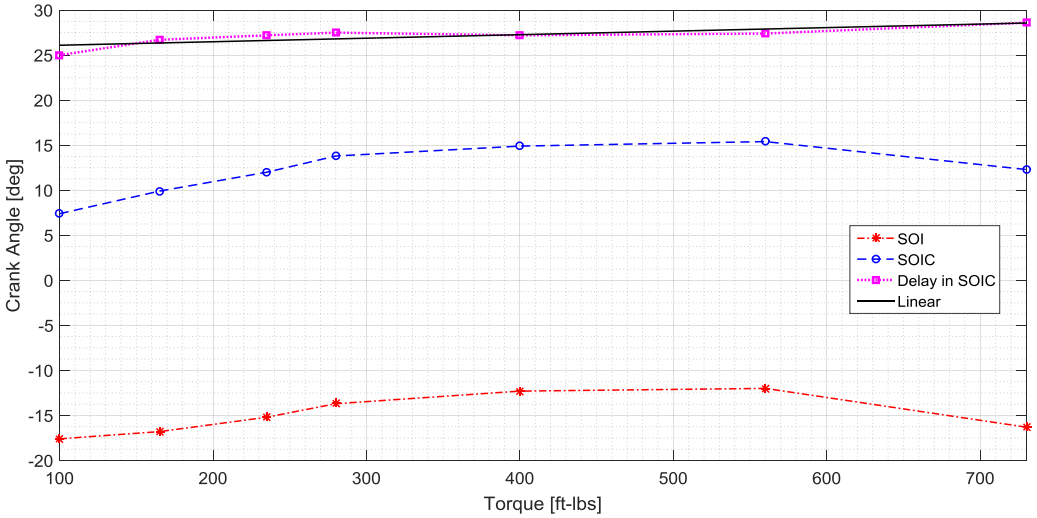

Figure 4.13: Delay in SOIC from SOI

Engine Load [ft-lbs]	SOI [CAD]	EOI [CAD]	Delay [CAD]
100	-17.6	-2.0	25.0
165	-16.8	1.5	26.7
235	-15.2	4.8	27.2
280	-13.7	7.3	27.5
400	-12.3	11.1	27.2
560	-12.0	14.6	27.4
730	-16.3	15.0	28.6

Table 4-2: Offset in SOIC from SOI

For the middle test points (165 to 560 ft-lbs), the delay between SOIC and SOI was 27.1 CAD +/- 0.35 CAD. However, if the lowest and highest test points are considered (100 to 730 ft-lbs), the spread increases sharply to +/- 1.8 CAD with a middle value of 26.8 CAD. It is believed that the increased spread in the SOIC delay with the lowest and highest test points can be attributed to the actuation of the HEUI system. In addition to the change in injection timing by the ECU, the actual start of injection is also influenced by the HEUI oil supply pressure. Based on engine speed and load, the HEUI injection pump internally changes displacement which in turn increases the oil supply pressure to the fuel injector. With

higher oil supply pressure, the opening of the fuel injector needle opens at a higher rate of speed. Although the change in oil supply pressure would offer an explanation in the change in SOIC delay, the expected trend is opposite of that which was observed. To truly build a correlation between SOIC and SOI, a modified fuel injector with needle lift sensor is required.

4.4.2 Effect of Engine Load on Ion Current

A sweep of engine loads was performed at a constant engine speed in order to determine the effect on ion current. At 1440 RPM, seven test points from 100 to 730 ft-lbs were chosen. From running this sweep, *Figure 4.13* shows that the amplitude of ion current increases with the increase in engine load. Although this figure also shows changes in the SOIC, this is a function of the different injection timings, not engine load.

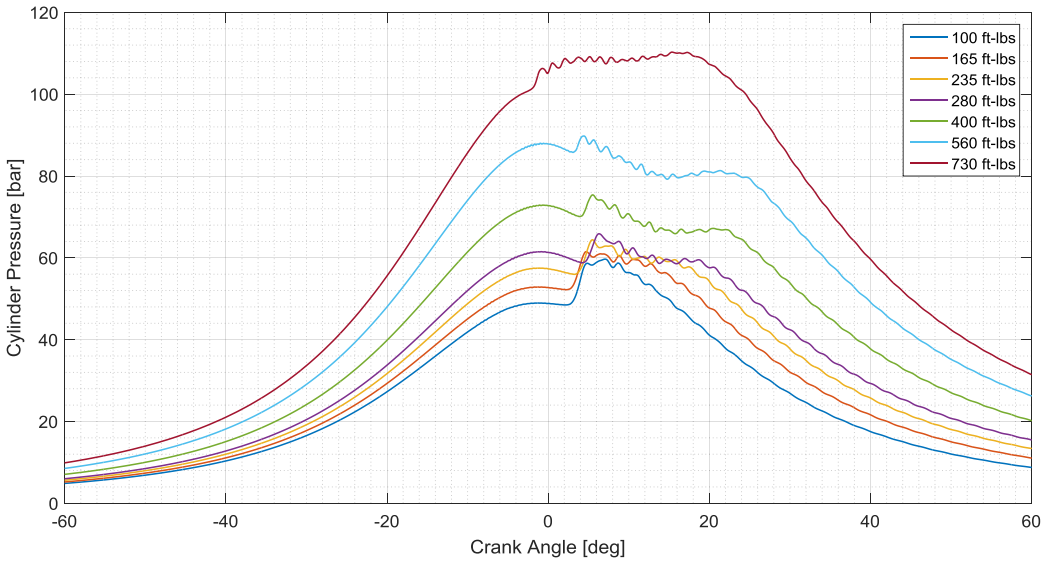

Figure 4.14: Change in Cylinder Pressure with Engine Load

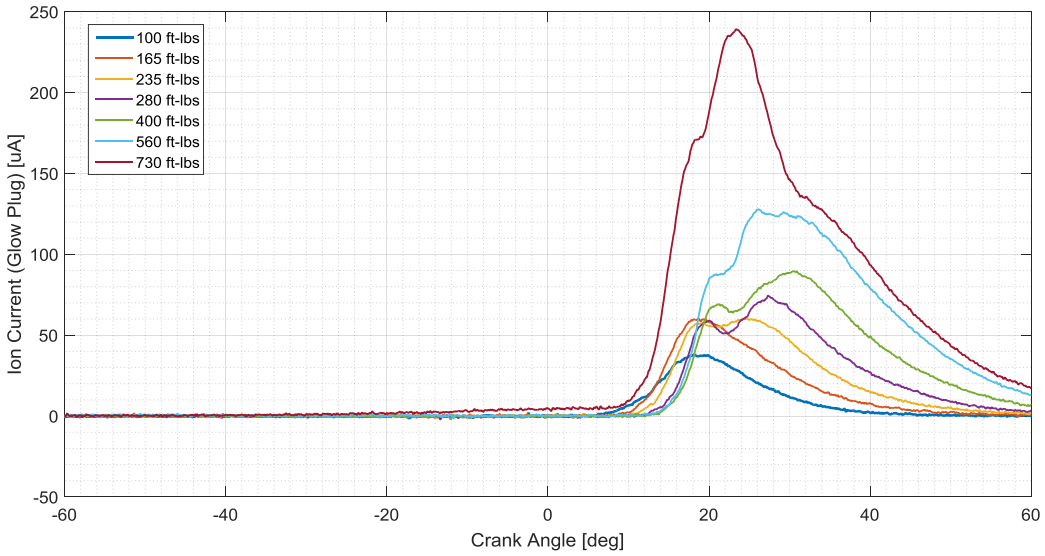

Figure 4.15: Change in Ion Current Amplitude with Engine Load

To illustrate the relationship between engine load and ion current amplitude, the amplitude of peak ion current was investigated. Since cylinder pressure increases with engine load, a comparison was made of peak cylinder pressure to peak ion current. This is shown in *Figure 4.16* and is fitted with a linear trend line. In order to describe the closeness of the fit of the linear trend line to the data, the coefficient of determination, R^2, was calculated and found to be 96.6%.

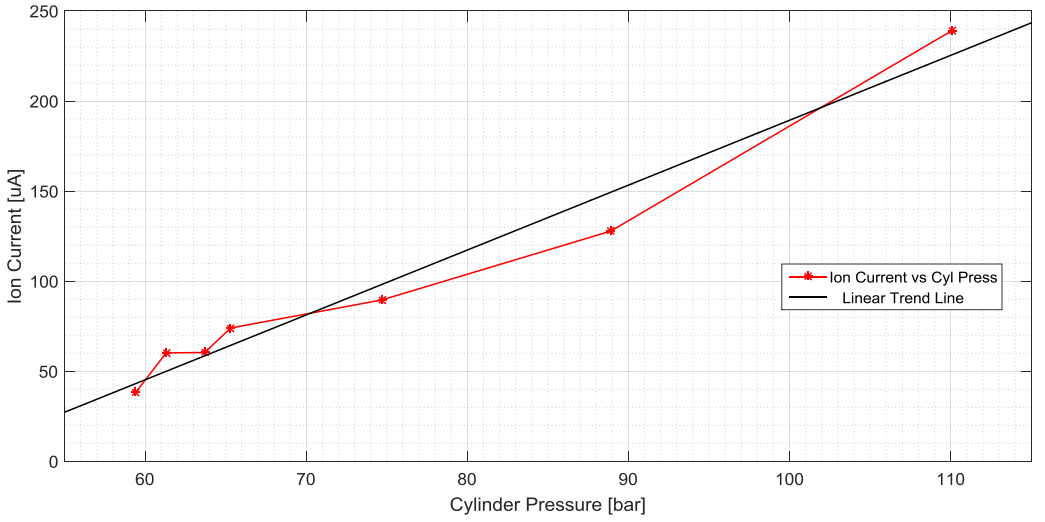

Figure 4.16: Relationship between Ion Current Amplitude and Cylinder Pressure

4.4.3 Comparison of SOIC to RHR

Although, earlier in this paper, it has been shown SOIC is related to the start of injection, it is also important to demonstrate the relationship between SOIC and actual combustion events. In order to be consistent with our significant publications in ion current research, LPPC (location of the peak of pre-mixed combustion) from the RHR of heat release was chosen. This is a term that Badawy [3] defined in his work. LPPC is the first peak in the RHR which signals pre-mixed combustion has occurred. *Figure 4.17* identifies the LPPC and shows the RHR curves for the ion current data collected by the glow plug.

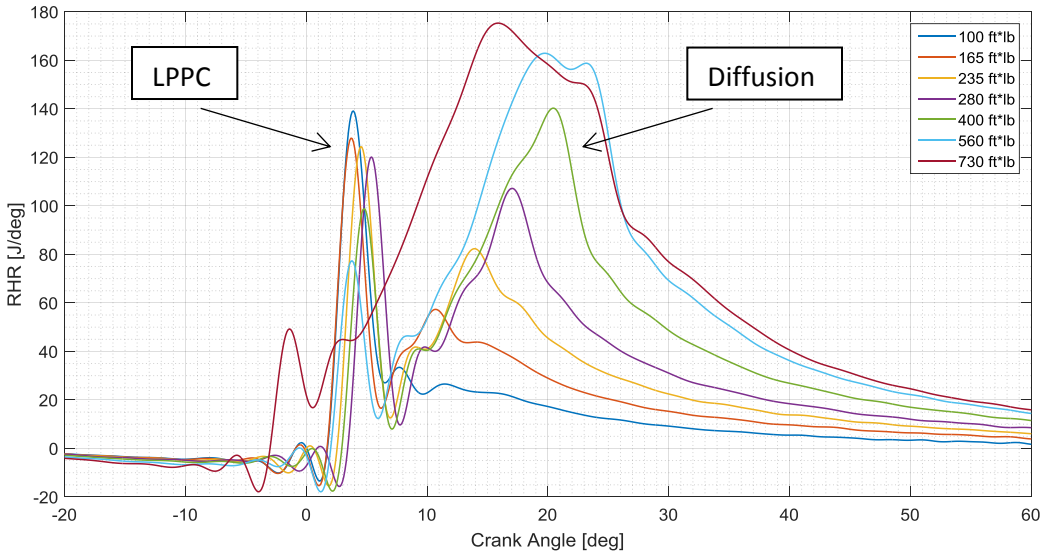

Figure 4.17 : RHR for Ion Current from Glow Plug

From *Figure 4.17*, there are a few important trends that can be identified. First, with increasing engine load, amplitude of the LPPC decreases. Looking back at *Figure 4.11*, this expected because the SOI was advancing towards TDC. This means that the amount of fuel in the combustion chamber at the start of combustion was less than low-load points with earlier SOI. Second, amplitude of the diffusion burn period increased with engine load. With SOI closer to TDC and injection duration increasing with engine load, the majority of the fuel is injected and burned later in the expansion stroke. This accounts for the higher diffusion burn at medium to high load points. Although the highest load point, 730 ft-lbs, also follows these two trends, its SOI was retarded to increase the injection duration without placing EOI too

late in the expansion stroke. *Figure 4.18* summarizes the trends of decreasing LPPC and increasing diffusion burn with increased engine loading.

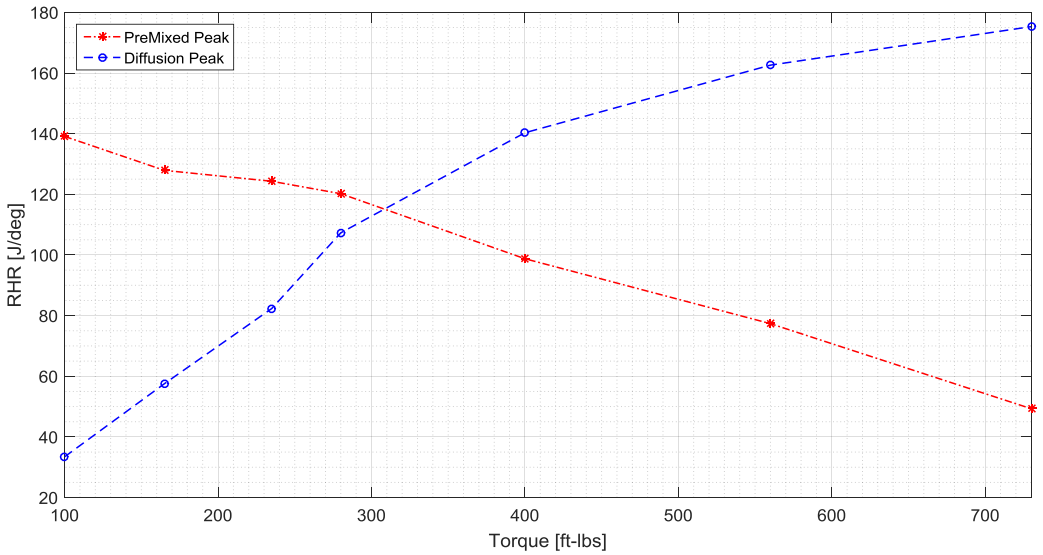

Figure 4.18: Amplitudes of LPPC and Diffusion Burn

In other ion current research, the delay between LPPC and SOIC has been 0.5-1 CAD [3]. However, in this experimental study, the delay between these two events was much greater. In addition, the delay steadily increased with increasing engine load. Although great care was taken in choosing a site for the ion current glow plug to avoid the fuel injector spray, it is believed that liquid fuel was wetting the sensing tip. This is reasonable since the delay is small at light loads where the EOI comes early. At high loads, a large delay is experienced since the longer injection duration pushes EOI deeper into the diffusion burn. *Figure 4.19* relates the delay of LPPC and SOIC to the EOI of the injection command.

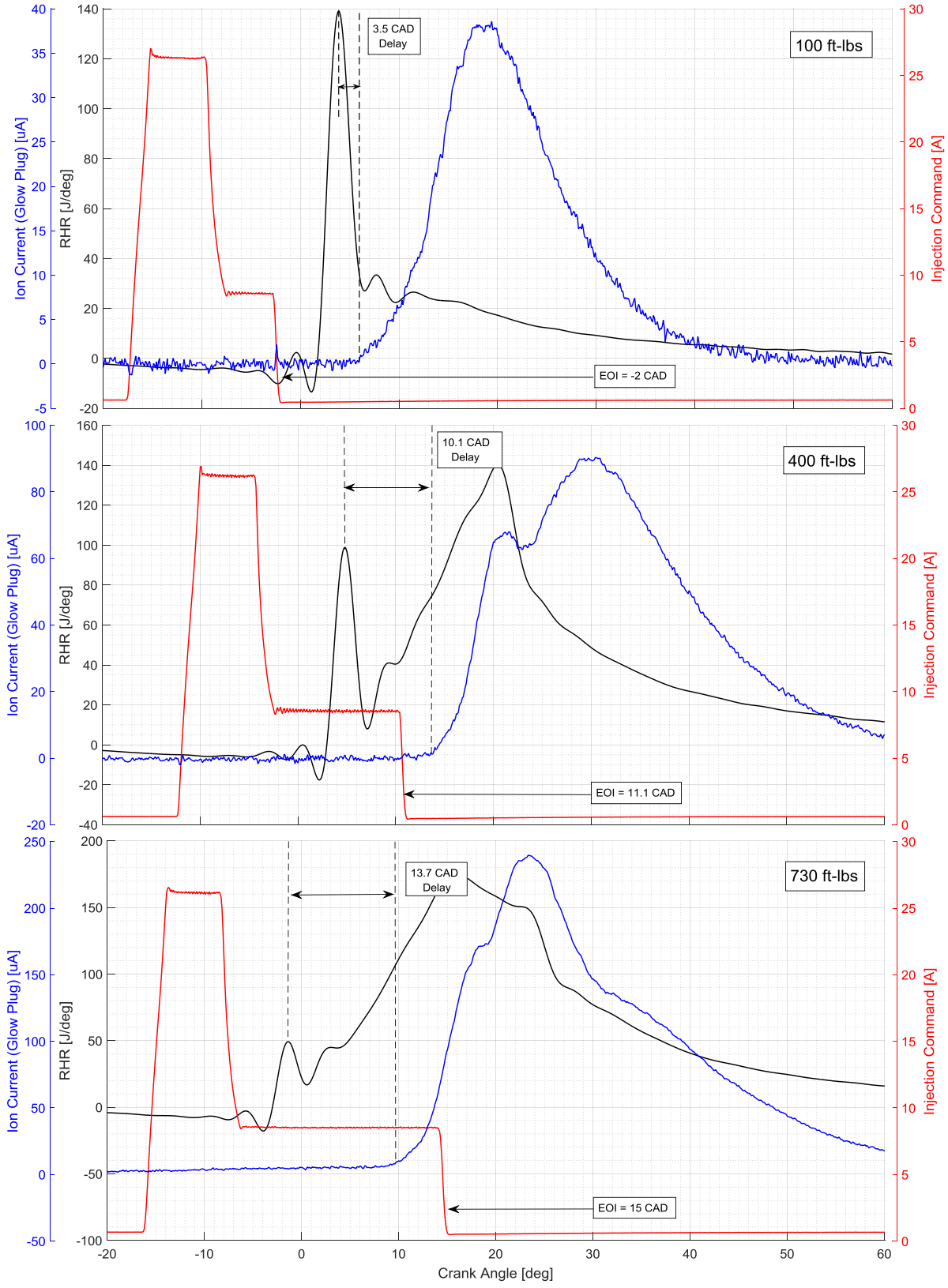

Figure 4.19: Increase of Delay Between LPPC and SOIC

Since SOI could not be held constant, the relationship between SOIC and LPPC had to made by comparing the delay in SOIC. *Figure 4.20* shows the SOIC, LPPC, and delay in SOIC at various engine loads. The delay in SOIC was fitted with a linear trend line. The coefficient of determination, R^2, was calculated and found to be 94.4%.

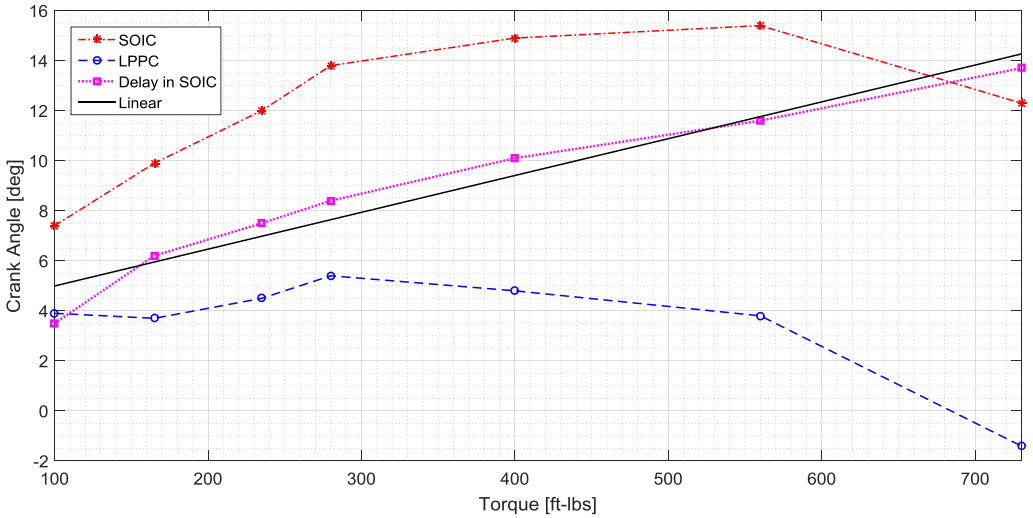

Figure 4.20: Delay in SOIC from LPPC

From *Figure 4.20*, it can be seen that the delay in SOIC steadily increases with increased engine load. This means that the LPPC and SOIC grow farther apart at higher loads. Since the rate of increase is was fairly constant, ion current signal can be used as a method to predict the timing of pre-mixed combustion. However, more work is needed to understand the effect of different engine speeds on this relationship.

CHAPTER 5.0 : CONCLUSION AND RECOMMENDATION FOR FUTURE WORK

In this work, experimental measurements were performed on a military, heavy-duty, diesel engine. The findings of these experiments are summarized by the following conclusions:

1. The detection of ion current on a HEUI injection system was demonstrated through both a modified fuel injector and modified glow plug. Although both ion current sensors produced an ion current signal, the glow plug produced the best results. Insulation issues with the ion current fuel injector sensor kept the results from being comparable.
2. In addition to sensing ion current in the combustion chamber, the ion current fuel injector detected the characteristics of the fuel injection command from the ECU. These characteristics include start of injection command, start of peak current, end of peak current, start of hold current, and end of hold current. From these events in the injection command, the ion current fuel injector can be used as diagnostic tool for the fuel injection system.
3. The time delay between the SOIC and SOI command was found to be constant regardless of injection timing or engine load. The time delay had very little variation in medium engine loads, but variation increased at light and heavy engine loads.
4. The amplitude of the ion current signal was shown to rise with cylinder pressure. Since cylinder pressure increases with engine load, a direct link between ion current amplitude and engine load can be made.
5. Ion current can be used as a method to predict the timing of pre-mixed combustion. The delay in SOIC from LPPC was measured and found to increase at a constant rate with increasing engine load.

Due to time constraints and failure of the ion current glow plug instrumentation sleeve, not all of the planned experiments were conducted. In future work, the following areas are recommended for investigation:

1. A method for filtering or shielding the ion current fuel injector from the injection command is needed. Although sensing the injection command is helpful as a diagnostic, the over run of the injection command into the detection of ion current from combustion poses a serious limitation. The ability to switch between modes of sensing the injection command and detecting ion current is needed in order to properly evaluate the HEUI fuel injector as a viable option as an ion current sensor.
2. The effect of multiple injections on the ion current signal has not been explored on a HEUI system. To test the sensitivity of the ion current response, sweeps of engine load at different engine speed need to be performed. This will demonstrate if multiple injections can be discerned from the ion current signal.
3. Variation in the time delay from SOIC to SOI command could be explained by oil actuation pressure or other HEUI system characteristics. The use of an instrumented fuel injector with needle lift sensor could detect the actual start of injection. This would reveal if the variation is explainable by HEUI system characteristics or is inherent to diesel combustion processes. Originally, an injector with needle lift sensor was planned for this effort, but it was damaged before it could be used to capture this information.

APPENDIX A

For the purpose of data analysis and simulation, the valve timing events for the engine were needed. Although this information was requested from Caterpillar, they were not able to share it since it was deemed proprietary. Because of this, the valve timings were measured manually. This was done by placing a dial indicator on the rocker arm of the intake and exhaust valves. The engine was then rotated slowly by hand. Marks were placed on the crankshaft pulley for at the different valve timing events. The angle between these marks was then measured using a 360 degree protractor. *Figure A.1* shows the dial indicator position on the rocker arm. *Figure A.2* displays the valve timing events on the crankshaft pulley. *Table A.1* lists the measured valve timing events.

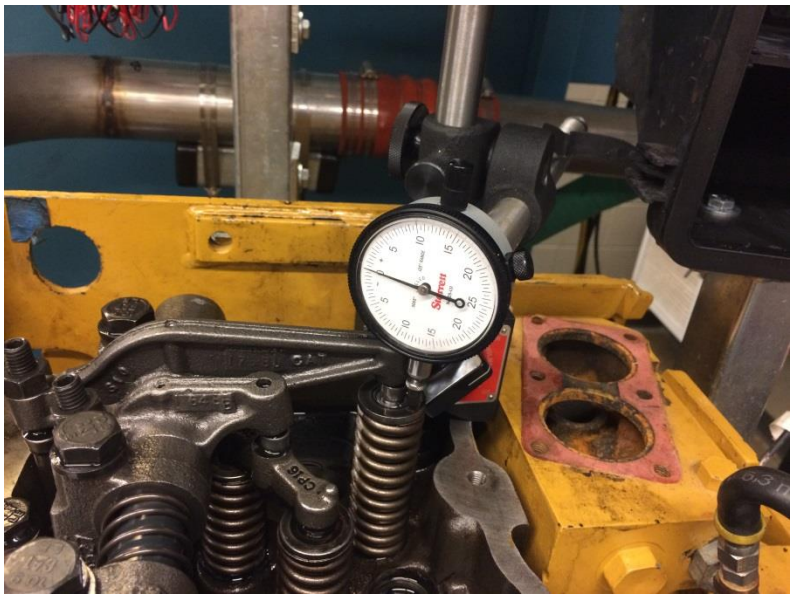

Figure A. 1: Position of Dial Indicator to Measure ValveTimings

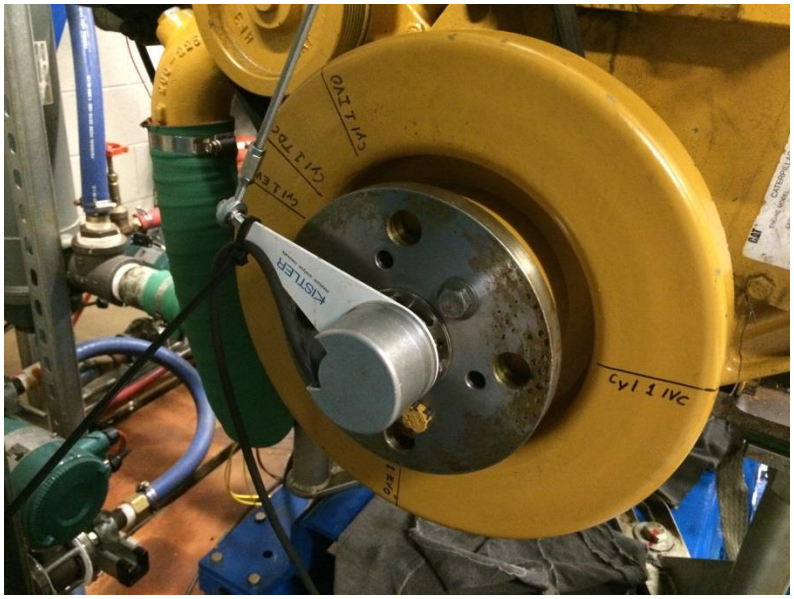

Figure A. 2: Labeling of Injection Timings Events on Crankshaft Pulley

Valve Event	Timing
EVO	59° BBDC
IVO	21° BTDC
EVC	13° ATDC
IVC	37° ABDC

Table A. 1

APPENDIX B

Product	Part Number	Reason for Failure
Glyptal Red Enamel	1201	Scratched off during installation
ToolMates Insulating Epoxy	401	Scratched off during installation
ToolMates Red Insulating Varnish	6084	Scratched off during installation
Permatex Muffler Tailpipe Sealer	80335	Could not apply even consistency
Permatex Muffler and Tailpipe Putty	80333	Could not apply even consistency
Permatex Exhaust Repair	80332	Could not apply even consistency
QuikSteel	Hi-Temp	Could not apply even consistency
FiberFix	80335	Too thick
PTFE Tape	76495A12	Wore through at medium engine loads
Ceramic Coating	NA	Cracked off during installation

Table A. 2: Unsuccessful Attempts to Insulate Fuel Injector

REFERENCES

1. Glavmo, M., Spadafora, P., and Bosch, R., “Closed Loop Start of Combustion Control Utilizing Ionization Sensing in a Diesel Engine,” SAE Technical Paper 1999-01-0549, 1999.

2. Kubach, H., Velji, A., Spicher, U., and Fischer, W.,“Ion Current Measurement in Diesel Engines,” SAE Technical Paper 2004-01-2922, 2004.

3. Badawy, T., Henein, N., Bryzik, W., “Closed Loop Control Using Ion Current Signal in a Diesel Engine,” SAE Technical Paper 2011-01-2433, 2011.

4. Badawy, T., Shrestha, A., Henein, N., “Detection of Combustion Resonance Using an Ion Current Sensor in Diesel Engines,” ASME J. Eng. Gas Turb. Power, Vol 134, 052802-1.

5. Estefanous, F., Henein, N., “Multi Sensing Fuel Injector for Electronically Controlled Diesel Engines,” SAE Technical Paper 2011-01-0936, 2011.

6. Henein, N., Badawy, T., Rai, N., Bryzik, W., “Ion Current, Combustion and Emission Characteristics in an Automotive Common Rail Diesel Engine,” ASME J. Eng. Gas Turb. Power, Vol 134, 042801-7

7. Peron, L., Charlet, A., Higelin, P., Moreau, B., Burq, J.F., “Limitations of Ionization Current Sensors and Comparison with Cylinder Pressure Sensors,” SAE Technical Paper 2000-01-2830, 2000.

8. Larsson, M., Denbratt, I., Koopmans, L., “Ion Current Sensing in an Optical HCCI Engine with Negative Valve Overlap,” SAE Technical Paper 2007-01-0009, 2007.

9. Fernandes, G, Fuschetto, J, Filipi, Z, Assanis, D, McKee, H Impact of military JP-8 fuel on heavy-duty diesel engine performance and emissions. *Proc. IMechE Part D: J. Automobile Engineering,* 2007, 221, 957-969.

10. Estefanous, F., Badawy, T., Henein, N., “Cycle Resolved In-Cylinder NOx and Ion Current Measurements in a Diesel Engine,” SAE Technical Paper 2013-01-0555, 2013.

11. Rai, Nilesh. “Measurement and Analysis of Ion Current Signal in an Automotive Common Rail Diesel Engine,” Master’s Thesis, Wayne State University, 2010.

12. Kurano, A., “Glow Plug with Ion Sensing Electrode,” U.S. Patent 5 893 993, Apr. 13, 1999.

13. Estefanous, F., “Multi-Sensing Fuel Injection System and Method for Making the Same,” Patent Application No. PCT/US10/42549, July 2010

14. Abdel-Rehim, A., Henein, N., VanDyne, E., “Ion Current in a Spark Ignition Engine Using Negative Polarity on Center Electrode,” SAE Technical Paper 2007-01-0646, 2007.

15. Abdel-Rehim, A., Henein, N., VanDyne, E., “Impact of A/F Ration on Ion Current Features Using Spark Plug with Negative Polarity,” SAE Technical Paper 2008-01-1005, 2008.

16. Kessler, M., “Ionenstromsenorik im Dieselmotor,” (PH.D. thesis), Fortsch-Ber. VDI Reihe 12 Nr. 487, Dusseldorf. VDI Verog, 2002.

17. Badawy, T., Estefanous, F., Henein, N., “Cycle-by-Cycle Soot Estimation in Diesel Engines,” SAE Technical Paper 2013-01-0545, 2013.

18. Glassey, S.F., Stockner, A.R., and Flinn, M. A., “HEUI – A New Direction for Diesel Engine Fuel Systems,” SAE Technical Paper 930270.

19. Coldren, D.R., Schuricht, S.R., and Smith III, R.A., “Hydraulic Electronic Unit Injector with Rate Shaping Capability,” SAE Technical Paper 2003-01-1384.

20. Caterpillar C7 Service Manual.

21. Bosch Diesel Fuel Injection Brochure, “Common Rail Systems CRS3 with 1,800 to 2,000 bar and Piezo Injectors,” 2012. http://www.boschautoparts.com

22. Caika, V., Kammerdiener, T., and Dorr, N., “Operation of Piezoelectric Common Rail Injector with Diesel and FT-Kerosene,” SAE Technical Paper 2007-24-0070.

23. Kohketsu, S., Tanabe, K., and Mori, K., “Flexibly Controlled Injection Rate Shape with Next Generation Common Rail System for Heavy Duty DI Diesel Engines,” SAE Technical Paper 2000-01-0705.

24. McGlothlin, M., “Inside the Bosch CP3 Injection Pump,” Diesel Power Magazine, 2012 http://www.dieselpowermag.com/tech/1204dp_inside_the_bosch_cp3_injection_pump/

25. Fisher, S., and Stein, Jens-Olaf, "Investigation on the Effect of Very High Fuel Injection Pressure on Soot-NOx Emissions at High Load in a Passenger Car Diesel Engine," SAE Technical Paper 2009-01-1930.
26. Abdullah, N.R., Rizalman, M., Rounce, P., Tsolakis, A., Wyszynski, M.L., and Xu, H.M., "Effect of Injection Pressure with Split Injection in a V6 Diesel Engine," SAE Technical Paper 2009-24-0049.
27. Ohishi, K., and Maeda, T., "The New Common Rail System for the Duramax 6600 V8 Diesel Engine," SAE Technical Paper 2001-01-2704.
28. Thirouard, M., Mendez, S., Pacaud, P., Chmielarczyk, V., Ambrazas, D., Garsi, C., Lavoisier, F., and Barbeau, B., "Potential to Improve Specific Power Using Very High Injection Pressure in HSDI Diesel Engines," SAE Technical Paper 2009-01-1524.
29. Carlucci, P., Ficarella, A., Chiara, F., Giuffrida, A., and Lanzafame, R., "Preliminary Studies on the Effects of Injection Rate Modulation on the Combustion Noise of a Common Rail Diesel Engine," SAE Technical Paper 2004-01-1848.
30. Tanabe, K., Kohketsu, S., and Nakayama, S., "Effect of Fuel Injection Rate Control on Reduction of Emissions and Fuel Consumption in a Heavy Duty DI Diesel Engine," SAE Technical Paper 2005-01-0907.
31. Fisher, B., and Mueller, C., "Effects of Injection Pressure, Injection-Rate Shape, and Heat Release on Liquid Length," SAE Technical Paper 2012-01-0463.
32. Zhang, L., "A Study of Pilot Injection in a DI Diesel Engine," SAE Technical Paper 1999-01-3493.
33. Badami, M., Mallamo, F., Millo, F., and Rossi, E.E., "Influence of Multiple Injection Strategies on Emissions, Combustion Noise and BSFC of a DI Common Rail Diesel Engine," SAE Technical Paper 2002-01-0503.
34. Osada, H., Uchida, N., Shimada, K., and Aoyagi, Y., "Reexamination of Multiple Fuel Injections for Improving the Thermal Efficiency of a Heavy-Duty Diesel Engine," SAE Technical Paper 2013-01-0909.

35. Atzler, F., Kastner, O., Rotondi, R., and Wiegand, A., “Multiple Injection and Rate Shaping, Part 1: Emissions Reduction in Passenger Car Diesel Engines,” SAE Technical Paper 2009-24-0004.

36. Estefanous, F., “Ionization is Diesel Combustion: Mechanism, New Instrumentation and Engine Applications,” Wayne State University Dissertation, 2011.

ABSTRACT

THE STUDY OF IONIZATION IN A MILITARY, HEAVY-DUTY, DIESEL ENGINE

by

STEVEN ZIELINSKI

December 2015

Advisor: Dr. Naeim Henein

Major: Mechanical Engineering

Degree: Master of Science

This thesis is an investigation of ionization in a military, heavy-duty, diesel engine. Ionization is a phenomenon which occurs in both spark-ignited and diesel engines. During the reactions of combustion, charged molecules and electrons are produced. The current produced, ion current, from these charges can be measured. The measurement of ion current can serve as an in-cylinder diagnostic for closed-loop engine control strategies. In this work, a literature review was performed to survey previous work as it pertains to ionization in diesel engines. In addition, a detailed description and comparison of the HEUI injection system was made to HPCR. This was done to give a fundamental understanding of the characteristics of the injection system which was employed in the research engine. Lastly, an analysis of experimental data provides insight as to the relationship between ion current and key combustion parameters.

AUTOBIOGRAPHICAL STATEMENT

Steven Zielinski graduated from Oakland University in 2011 with a Bachelor of Science in Engineering Physics. His professional career began in June 2010 with an internship for the US Army at TARDEC (Tank Automotive Research Development Engineering Command). This internship transitioned into full-time employment in 2011 when he joined GVPM (Ground Vehicle Power and Mobility). This division of TARDEC is responsible for the testing and evaluation of military vehicles and their powertrain components. In 2011, he began graduate studies at the University of Michigan and Purdue University through online programs. He continued his studies in 2013 by transferring to Wayne State University to conduct research in the CAR (Center for Automotive Research) under Dr. Naeim Henein. In 2014, he was co-investigator for an US Army ILIR (Independent Lab Independent Research) award on the topic of "Ionization of Combustion Gases in Military Diesel Engines". This topic was the focus of his research while pursuing his Masters of Science in Mechanical Engineering. Presently, he serves as the lead test engineer for US Army's Power and Energy Vehicle Environmental Laboratory.